Fall 2018

Geometric Optimization of a Heaving Point Absorber Wave Energy Converter

Ian Riley

GEOMETRIC OPTIMIZATION OF A HEAVING POINT ABSORBER WAVE ENERGY CONVERTER

by

Ian Riley

(Under the Direction of Marcel Ilie)

ABSTRACT

Wave energy shows significant potential for development into a competitive renewable energy source. Non-renewable resources are finite and contribute to adverse effects on the environment. Development of wave energy conversion devices that use heave motion as the primary driver for converting wave energy into electrical potential is explored through optimizing the geometry of an axisymmetric partially submerged buoy in deep water. The governing equations of motion and hydrodynamic forces are solved for in one degree of freedom using ANSYS Aqwa. An external PTO device is simulated to induce power capture in the system. Four different geometric shapes are tested and the introduction of supplemental mass and optimization of the hydrodynamic parameters across multiple sea states is conducted to determine the benefits of buoy shape selection. Time-averaged and peak power output is determined to be more than 10% higher in buoys of different shapes when compared to a cylindrical buoy, when tested in regular waves using the principles of linear wave theory which has shown good agreement with previous experimental results. Further testing of the different shaped buoys using the optimized supplemental mass and external PTO forces is examined in irregular waves but no correlation to the regular wave testing is determined, requiring a need for further study with irregular waves and CFD analysis.

INDEX WORDS: Wave energy, Hydrodynamic parameters, Aqwa, Renewable, Optimization, Buoy geometry, CFD

GEOMETRIC OPTIMIZATION OF A HEAVING POINT ABSORBER WAVE ENERGY CONVERTER

by

IAN RILEY

B.S., University of Maine, 2003

M.S., Georgia Southern University, 2018

A Thesis Submitted to the Graduate Faculty of Georgia Southern University

in Partial Fulfillment of the Requirements for the Degree

MASTER OF SCIENCE

STATESBORO, GEORGIA

GEOMETRIC OPTIMIZATION OF A HEAVING POINT ABSORBER WAVE ENERGY CONVERTER

by

IAN RILEY

Committee Chair: Marcel Ilie
Committee: Mosfequr Rahman
David Calamas

Electronic Version Approved:
December 2018

DEDICATION

To my father, Dr. John Graham Riley.

ACKNOWLEDGMENTS

To my wife Bobbie and my children, Chelsea, Caleb, Colby, and Corbin. Always my inspiration, motivation, and support system. Without you none of this would be possible. Also, to my advisor, Dr. Marcel Ilie for his guidance and direction, and to my mother Ruth Shaw and my sister Johanna Evans for their contributions.

TABLE OF CONTENTS

Page

LIST OF TABLES

Page

LIST OF FIGURES

Page

NOMENCLATURE

γ	Specific Weight	a	Amplitude
ρ	Density	F_e	Excitation Force
p	Pressure	ω	Angular Velocity
h	Depth	L	Capture Width
φ	Velocity Potential	C_{wr}	Capture Width Ratio
η	Water Surface Elevation	ω_n	Natural Frequency
g	Gravity	m	Mass
λ	Wavelength	A_{wp}	Cross Sectional Area
WEC	Wave Energy Converter	PTO	Power Take Off
LCOE	Levelized Cost of Electricity	T_p	Peak Wave Period
H_s	Significant Wave Height	J	Energy Flux
P	Power	F_b	Buoyancy Force
V_d	Volume of Displaced Fluid	b	Hydrostatic Damping Coefficient
t	Time	k	Wave Number

CHAPTER 1

INTRODUCTION

1.1 Energy needs of a developing world

Since the dawn of man, humans have sought to harness the power of the natural resources that abound on Earth for the purposes of heat, light, protection, transportation, innovation, and industry. The need for natural resources has continuously increased, especially as humans have become more sophisticated and dependent upon energy. This has inevitably led to heated debates, fighting, and sometimes war. Until the last half of the 21st century, disputes over natural resources were often circumvented through the development of new technology to harvest more resources or the relocation and expansion of peoples to new uninhabited areas. In the end, the supply and demand relationship appeared, for all intents and purposes, to be in balance.

As the new millennium approached however, a harsh new reality came into focus for much of humanity. It was apparent that the demand for energy was indeed beginning to outstretch supply. To better understand this increase in demand, it has been estimated that the energy consumption of pre-historic man for heat and light was estimated to be about 2,000 kcal per capita, whereas by the late 1900s, it was estimated that energy consumption had increased by more than 10,000% compared to those first civilizations [8].

The production of the energy required to sustain the world's ever-growing need has relied primarily on the burning of fossil fuels. As scientists discovered more about the limitations and finite amounts of fossil fuels [44], the conversation began to shift in a profound way towards what might happen if the country ran out of fossil fuels. The problem being presented to scientists and engineers today is how to approach this ever-increasing imbalance when discussing energy. There are many unanswered questions. *When will these resources run out? What other options are out there? What are the long-term impacts of these choices?* These questions are more relevant today than ever before and as such have been shifted to the forefront of scientific discussion.

1.2 Energy consumption and determining factors

According to the Lawrence Livermore National Laboratory (LLNL), in 2017 the United States consumed an estimated 97.7 quadrillion BTUs (quads) of energy, or 2.86 x 10^{13} kilowatt-hours [38]. Of that, only 31.1 quads were consumed as useful energy, that is, work done by machines, heat for homes, etc. The remaining 66.7 quads were classified as rejected energy. What this means is that of all the potential energy that was extracted through various means from both renewable and non-renewable sources only about a third of it was captured. The goal of increasing the efficiency of electricity production is a field of research all on its own and increases in efficiency could go a long way to reducing the amount of resources being used. The Sankey Diagram for Energy Consumption is provided here in Figure 1 courtesy of LLNL and the Department of Energy [38].

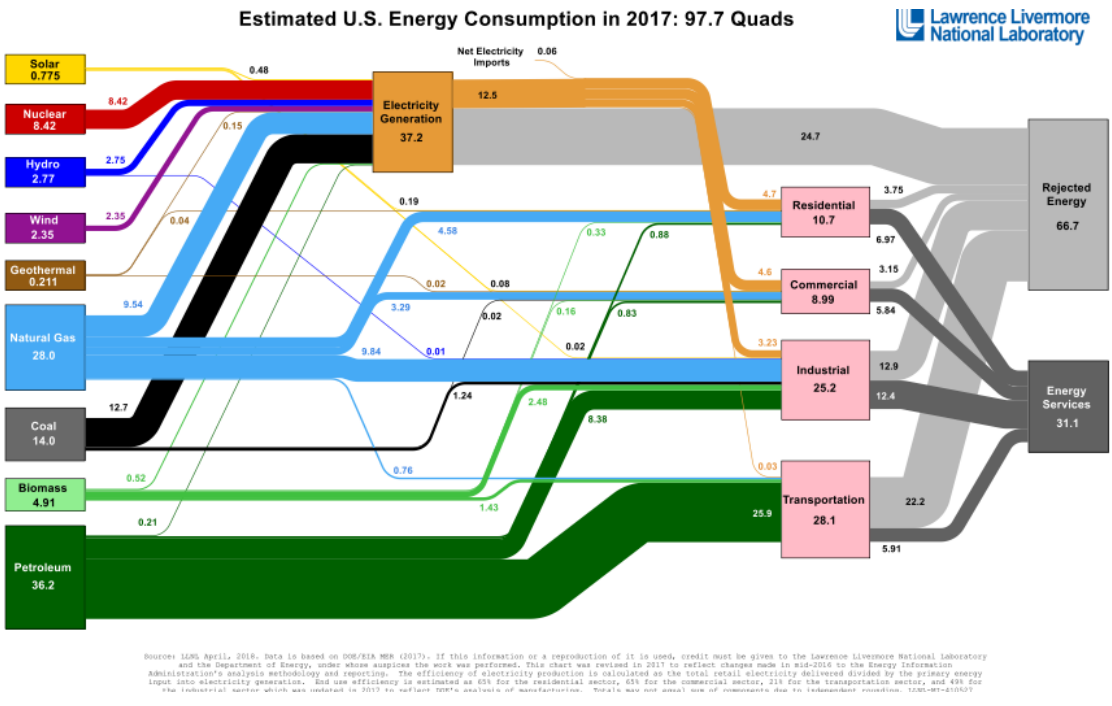

Figure 1. U.S. energy flowchart [38]

What is depicted in Figure 1 is the total amount of energy consumed in the United States in 2017. It is divided by the type of resource on the left, both renewable and non-renewable. Each of the resources then is split between different consumers of energy, like electricity and transportation. At the outlet of each consumption activity a portion of the energy is going to the energy service (work) and the rest to rejected energy or waste heat based on the efficiency of each activity.

There are two factors causing an increase in global energy consumption, even with the improvements in efficiency of many devices: the worldwide population is increasing, and the per capita usage is increasing. For example, according to the U.S. Census Bureau, the population of the United States in 2017 was 326,965,105 [39]. The United Nations 2017 "World Population Prospects" report indicates that the U.S. population is expected to increase as much as 38% over the next 80 years up to nearly 450 million people [40]. Even if the assumption is that energy consumption remains the same per capita, making no changes to consumption rates, the estimated energy consumption for the U.S. in the year 2100 based upon this projected population would be 134 quadrillion BTUs.

However, to make the problem worse, as populations of countries around the world improve their quality of life, energy consumption per capita also increases. According to John Fanchi, using the United Nations Human Development Index (HDI), where 0 indicates no quality of life and 1 is a very high quality of life, the energy consumption tapers off at an HDI of about 0.8 to approximately 200,000 MJ per capita [8]. In the 2016 United Nations Human Development Report, the United States ranked 10th out of 188 countries with an HDI of 0.920. On the same report, there are almost 100 countries which fall below an HDI of 0.7 [41]. It would not be too presumptuous to believe that these countries will aim to improve their quality of life over time. This results in additional increases in energy consumption worldwide over the next century based on increases in quality of life due to the subsequent per capita energy increase, independent of population size. This HDI index is presented as an indicator to correlate the increase in energy use to the increase in quality of life that all nations strive for. The U.S. consumption of energy may be directly or indirectly impacted by this global increase.

The predicted population growth and increase in quality of life described here are the primary drivers for an increase in the demand for energy. As the name implies, non-renewable resources are finite. In order to estimate the amount of time it will take to fully deplete non-renewable resources, researchers must gain an understanding of the limited amount available. In 1973 the United States experienced the deleterious effects of the Arab oil embargo [12]. Although these events were primarily politically driven events, it served as a wake-up call for everyday Americans who ended up waiting in gas lines for much longer than expected only to find that U.S. production couldn't make up for the 20% cut in imports. It became widely believed that the U.S. was critically dependent on non-renewable, imported natural resources for day-to-day activities.

Despite oils limited role in total electricity generation — around 1 percent — its direct impact on the transportation industry was felt by every American and political pressure intensified for the U.S. Government to step in. As a result, President Jimmy Carter created what is now known as the U. S. Energy Information Administration (EIA). According to their mission statement, the EIA "collects, analyzes, and disseminates independent and impartial energy information to promote sound policymaking, efficient markets, and public understanding of energy and its interaction with the economy and the environment" [44]. The role of the EIA evolved to encompass more than just the transportation industry and oil reserves, and now serves as the primary governmental agency for estimating natural resources.

1.3 The condition of America's energy portfolio

To narrow the scope of the developing problem, the electricity generation as defined in the Sankey diagram (Figure 1) is examined in more detail. To delineate the relative production percentage provided by different energy resources, the pie chart in Figure 2 makes clear that more than 75% of electricity production comes from only three sources- coal, natural gas, and nuclear- all of which are non-renewable

in nature, and current energy production levels from these sources are orders of magnitude higher than any other production source.

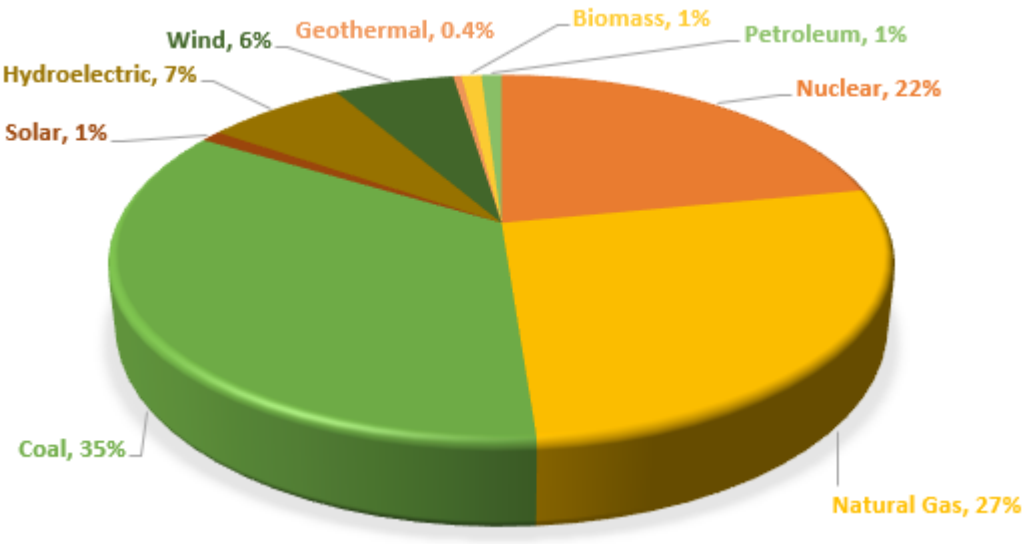

Figure 2. U.S. electricity production by type, 2017

Due to the dominance of coal, natural gas, and nuclear power in the energy market, those are the non-renewable resources that are examined in further detail. As of 2018, according to the EIA, the U.S. has 254 billion short tons of recoverable coal reserves, that is, the amount of coal that "can be mined with today's mining technology after considering accessibility constraints and recovery factors" [44]. That amount of coal is estimated to last for 348 years. The EIA does not publish whether this accounts for variables like population growth, but references the estimate based on current U.S. coal production. It is difficult to make predictions on future exploration of possible untapped coal reserves or improvements which could lead to higher efficiency, thus prolonging the usefulness of the available coal. As of 2017, there were no new coal power plants scheduled for production, but recently coal has had a spotlight on the national stage and its resurgence may lead to higher yields, or faster depletion, or both.

The amount of natural gas is also studied by the EIA. The agency estimates that "as of January 1, 2015, there were about 2,355 trillion cubic feet (tcf) of technically recoverable resources of dry natural gas in the United States" [44]. Based on current consumption rates, EIA estimates that quantity will last for about 86 years. However, it is interesting to note that in 1976, the scientist M.A. Styrikovich of the Academy of Sciences of the USSR estimated, based on 1976 consumption rates, there would be no more natural gas by 1995 [13]. This historical estimate from over 40 years ago is so vastly different from what estimates are now that it is reasonable to say that estimates will continue to change as new methods of discovery are implemented and technological resources improve.

The third and perhaps most controversial of the top energy sources for electricity production is nuclear power. According to the EIA, uranium is the most common fuel used by nuclear power plants to produce electricity. Of the 50.6 million pounds of uranium purchased by the U.S., 89% of it was imported from other countries [44]. Additionally, the Nuclear Energy Association estimates the Earth's uranium resources at approximately 16 million metric tons, discovered and projected. This has the potential, based on today's technology, to last for 230 years. This estimate does not account for other methods of producing nuclear energy but does represent the majority of nuclear production.

1.4 Adverse impacts of non-renewable energy sources

Aside from the politics of free trade, the entanglements of foreign reliability on oil, and the potential for new resources to be discovered, non-renewable resources may be exhausted within the next ten generations based on the information currently available. However, there are additional reasons to consider placing more emphasis on developing renewable energy sources. It has become increasingly clear to not only environmentalists, but to the mainstream public, that there is evidence that the burning of fossil fuels and release of pollutants into the atmosphere is causing global warming, the impacts of which are being debated on the world stage today.

In support of this position, data from the Vostok ice core in Antarctica shows that CO_2 levels have fluctuated over the last 400,000 years and over that timespan the rising CO_2 levels are indicative of global increases in temperature [1]. Figure 3 shows the levels of CO_2 found in the ice core. The highest levels recorded were around 300 ppmv (parts per million by volume). Similar results were obtained from other ice cores to validate the study. It has been found recently though that CO_2 levels have been increasing since the 1950s at never before seen levels and according to NASA, in 2013, CO_2 levels reached 400 ppmv [24]. This evidence supports the premise that there has been an increase in the amount of CO_2 in the atmosphere above the traditional fluctuations, and that there may be a correlation to the advent of the industrial revolution because of the increase in the burning of fossil fuels.

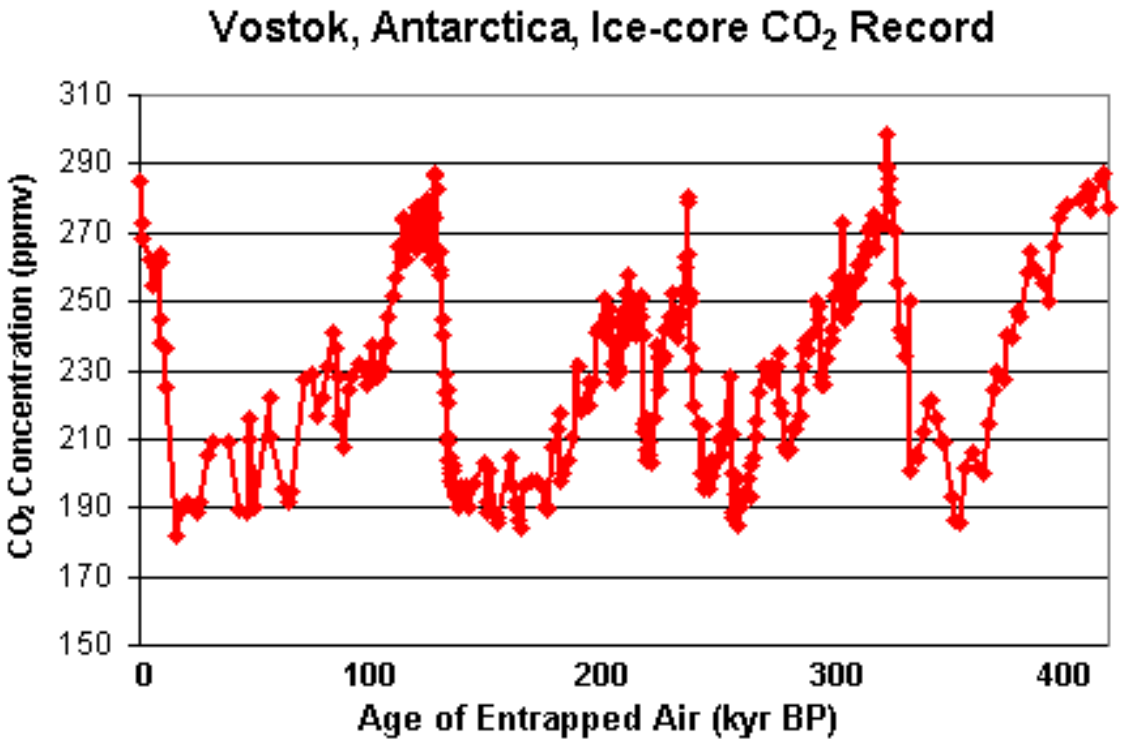

Figure 3. CO_2 levels from the Vostok ice core in Antarctica for the past 400,000 years [1]

This evidence, along with what is known about the current state of energy production and consumption, population growth, quality of life, and available resources, indicates that humanity is readily approaching an energy crisis. Additionally, it is clear from this discussion that there is a need to increase the production of non-fossil fuel-based energy to meet the global demands of the future.

1.5 The transition to renewable energy

With the advancement and increased availability of solar, wind, and geothermal technology over the last 30 years, a fledgling movement to begin the transition from non-renewable fuels to renewable energy sources has begun to take root in American industry, culture, and to some extent, politics. Looking back at Figure 2, it is apparent that wind and solar resources have a small foothold as part of the energy supply. The shift to renewable energy sources seems only logical given the facts presented above, but there are a number of significant technical challenges that have yet to be overcome.

To better understand the options for transitioning from non-renewable fuels to renewable energy sources, the resources for producing renewable energy must be identified, the advantages and costs explored, and a path determined for how to decide what is the best option or combination or options. The researchers Bent, Bacher, and Thomas define renewable energies as, "hydroelectric power generation, solar thermal energy, the direction conversion of solar energy to electrical energy (photovoltaic energy), wind energy, the capturing of the sun's energy in biomass, ocean thermal energy conversion, wave energy, geothermal energy, and tidal energy" [2].

Each of the methods currently available for producing renewable energy sources has advantages and disadvantages. The usefulness of hydroelectric power generation, for example, has been taken advantage of for many years because of the simple nature of the method and the availability of the flowing water of rivers across the country. Some benefits include the huge amount of energy that can be extracted by inserting a large dam into a waterway to create significant potential in the form of a giant lake and then

passing the high-pressure water through large turbines. However, what has been learned over the years is that interrupting the natural flow of rivers as they make their way from the mountains to the sea can be extremely disruptive or even life threatening to various animal species. Additionally, creating man-made lakes certainly benefits the recreation industry for fishing and boating, but at the same time, the aging infrastructure that supports these dams puts towns and villages at risk when there is potential for catastrophic failure and flooding.

Of all the renewable energies the two resources that have seen the most growth in recent years have been wind and solar energy (photovoltaic). The reasons for this are many, but perhaps the biggest factor at present is the reduction in what is called the Levelized Cost of Electricity (LCOE). According to the EIA, "Levelized cost of electricity (LCOE) is often cited as a convenient summary measure of the overall competiveness of different generating technologies. It represents the per-megawatt hour cost (in discounted real dollars) of building and operating a generating plant over an assumed financial life and duty cycle" [45]. Figure 4 shows the LCOE of several different energy sources, with a lower number representing lower cost. This figure shows that the LCOE of solar and on-shore wind power is currently estimated to be less than that of natural gas, nuclear, and hydroelectric.

Plant type	Capacity factor (%)	Levelized capital cost	Levelized fixed O&M	Levelized variable O&M	Levelized transmission cost	Total system LCOE	Levelized tax credit[2]	Total LCOE including tax credit
Dispatchable technologies								
Coal with 30% CCS[3]	NB	NB	NB	NB	NB	NB	NA	NB
Coal with 90% CCS[3]	NB	NB	NB	NB	NB	NB	NA	NB
Conventional CC	87	13.0	1.5	32.8	1.0	48.3	NA	48.3
Advanced CC	87	15.5	1.3	30.3	1.1	48.1	NA	48.1
Advanced CC with CCS	NB	NB	NB	NB	NB	NB	NA	NB
Conventional CT	NB	NB	NB	NB	NB	NB	NA	NB
Advanced CT	30	22.7	2.6	51.3	2.9	79.5	NA	79.5
Advanced nuclear	90	67.0	12.9	9.3	0.9	90.1	NA	90.1
Geothermal	91	28.3	13.5	0.0	1.3	43.1	-2.8	40.3
Biomass	83	40.3	15.4	45.0	1.5	102.2	NA	102.2
Non-dispatchable technologies								
Wind, onshore	43	33.0	12.7	0.0	2.4	48.0	-11.1	37.0
Wind, offshore	45	102.6	20.0	0.0	2.0	124.6	-18.5	106.2
Solar PV[4]	33	48.2	7.5	0.0	3.3	59.1	-12.5	46.5
Solar thermal	NB	NB	NB	NB	NB	NB	NB	NB
Hydroelectric[5]	65	56.7	14.0	1.3	1.8	73.9	NA	73.9

Figure 4. Levelized Cost of Electricity for different energy technologies [45]

These estimates do not include coal because at the time of publishing there was no planned construction for coal fired power plants. However, according to the Institute of Energy Research, existing coal plants fall on the low end of cost when compared to other technology [45]. One of the primary influences on the future of new renewable energy technology development will be whether the LCOE can be reduced to a point where developing and marketing renewable energy resources is financially viable for companies to take on as a serious investment. If there is no money to be made, investors may continue to avoid it.

1.6 Wind energy

Wind power has had a place in society since long before the idea of fossil fuels. As far back as the 20th century B.C.E. there have been examples of windmills being used to capture wind energy for water pumps [3]. Evidence of early windmills still exists today in Holland and wind farms are popping up across regions of the United States. The National Renewable Energy Laboratory recently published data that suggests if wind turbines were erected in non-environmentally protected areas, the wind resource in the United States would be 37 million gigawatt-hours, or 126 quads. Storage, transportation, efficiency, and other factors aside, this is more than the amount of energy consumed by Americans each year [47]. A map showing the wind potential at 80m high – the average height of a wind turbine – in the U.S. is seen here in Figure 5.

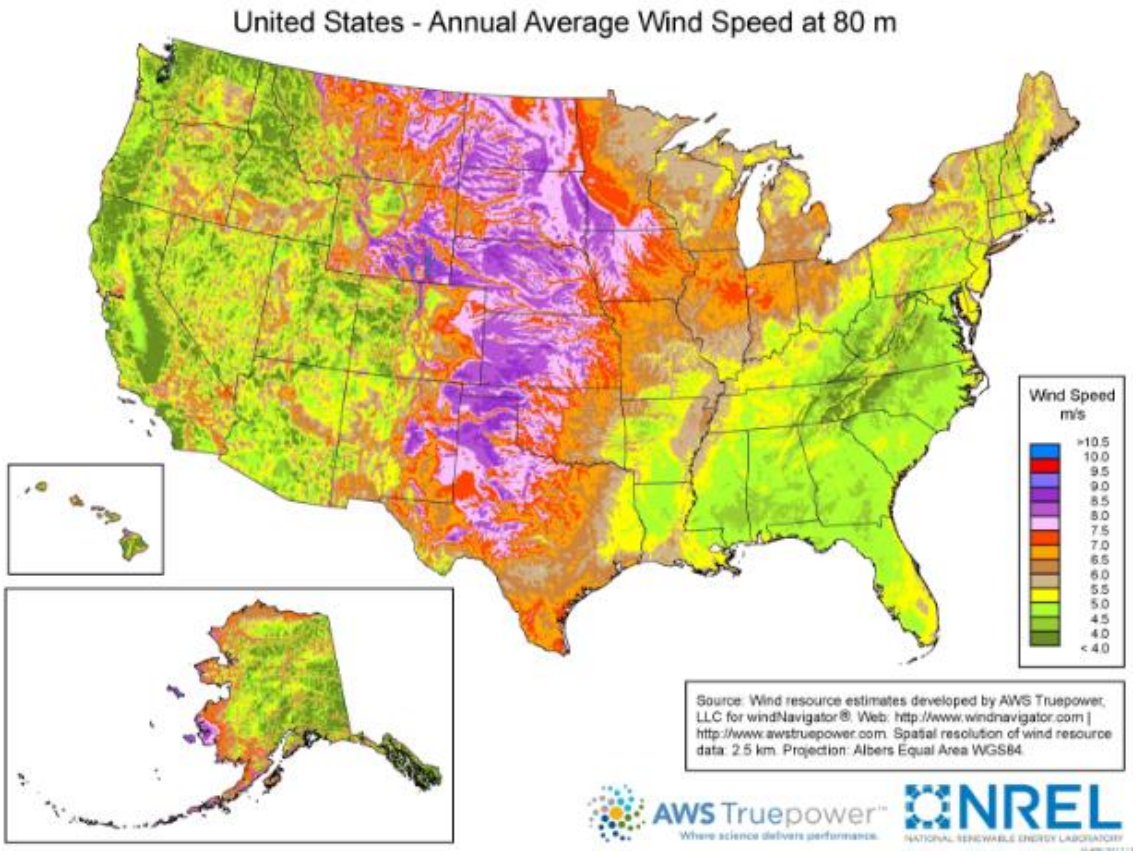

Figure 5. Average wind speed across the United States [43]

Although a viable resource, wind power has disadvantages too. Wind is inconsistent over time and not necessarily of the strength desired where there is high population density. As shown in Figure 5 above, the mid-west tends to have much higher average wind speed compared to areas such as the southeast [43]. The amount of acreage that is required by wind farms is significant, although efforts are being made for co-use of the land to include agricultural purposes [3]. Additionally, the visual impact on the countryside is not without serious consequence. The idea of replacing beautiful vistas with tracts of land dedicated to massive wind farms may not be worthwhile to some. Other down sides have been noted by environmentalists to include increased danger to birds and noise pollution, but those risks are fairly low and mitigation strategies are being developed to further reduce the risk. As part of a larger energy portfolio, continued advances in wind power will result in a reduction in fossil fuel consumption.

1.7 Solar energy

Solar power, a relatively new addition to the alternative energy mix, has seen a gradual increase in popularity and use in mainstream devices. There are solar powered cars, home heating units, cell phone chargers, and all manner of devices. First discovered in 1876, the ability of selenium cells to produce electricity when exposed to sunlight was thought to be technology that would change the world [46]. Over 100 years later, solar power only makes up 1% of the energy portfolio (see Figure 2).

The potential for solar power in the United States is quite significant. In parts of the southwest, 100,000 square feet of solar panels could provide enough energy to power 1,599 homes [46]. Figure 6 is a solar map from NREL that shows the variation in solar potential across the U.S.

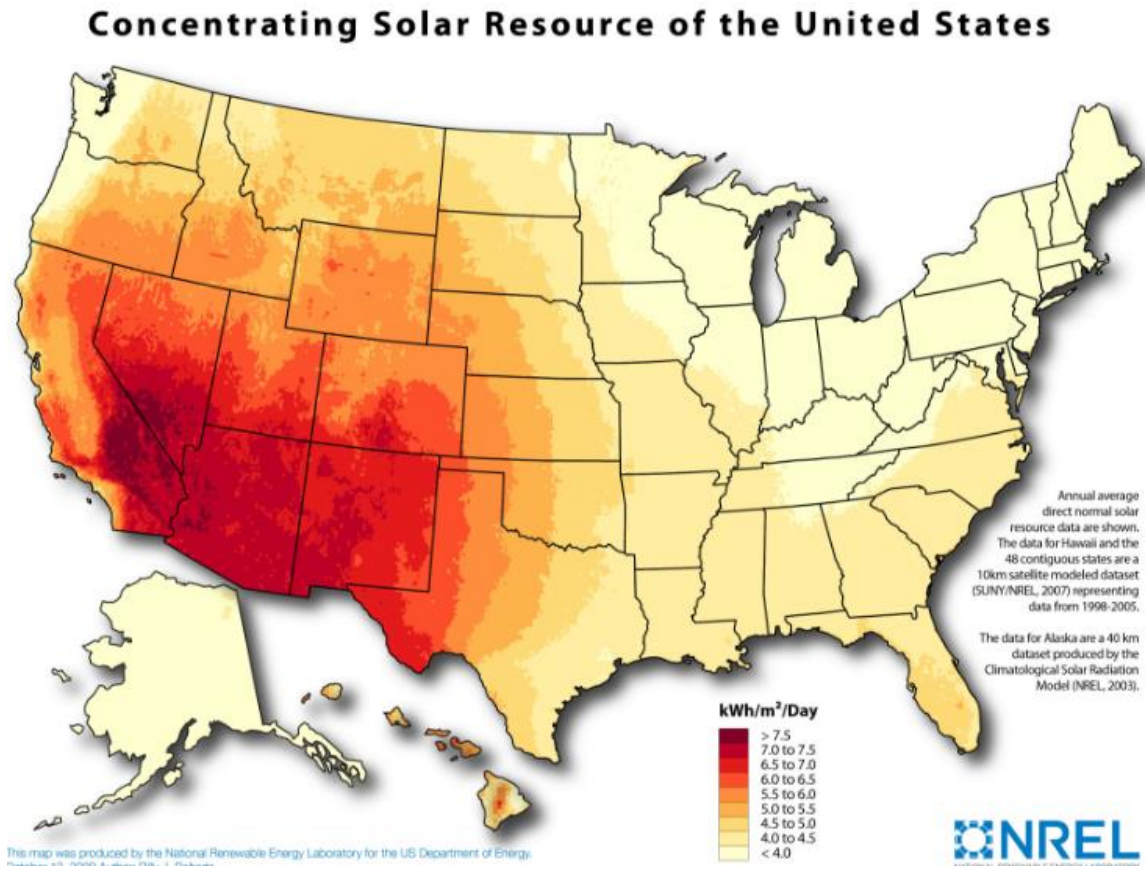

Figure 6. Solar potential across the United States [42]

Solar, like other resources, has its limitations. It is dependent on the sun shining so cannot produce at night, or on cloudy days, and certain regions like the Pacific Northwest just don't have a lot of sun. The initial cost can be quite high, although prices have been dropping considerably over the past decade, and maintenance costs are almost none because there are no moving parts. There is a significant land resource required, although there are efforts being made to develop co-use solar farms similar to wind farms. Additionally, solar panels can be mounted to rooftops, and even be made into roofing tiles. A major downfall however, is the waste that results from used solar panels. According to a recent study by Environmental Progress, an environmental policy non-profit agency, solar panel waste produces "300 times more toxic waste per unit of energy than nuclear power plants" [16]. Through further research and risk mitigation strategies, solar, along with wind can provide a viable addition to the energy portfolio. But as the reader will infer, no single strategy will resolve the impending energy crisis.

1.8 Ocean energy

To make a noticeable impact on the renewable energy landscape, exploration and development of all the available resources must be pursued. One renewable resource that has not been discussed yet is ocean renewable or marine renewable energy. The ocean can provide power from its currents and tides, temperature and salinity gradients, and, the topic of this thesis, wave power. Two-thirds of the planet is covered by ocean with intermittent waves that are a potential source of energy just waiting to be captured. It has been estimated by Professor John Sheffield of Purdue University that the power potential of wind waves in deep water of more than 100m is more than 7,500 Mtoe/a ($1x10^6$ tons of oil equivalent per year) [2]. That converts to approximately 300 quads/year, nearly twice as much energy used for electricity in 2007 worldwide [38]. Another estimate by G. Mørk, et al. puts the theoretical wave potential at 32PWh/year, which converts to 109 quads, just one third of the Sheffield estimate [22]. This variability in power potential is significant, however, the application of the data can still be utilized by focusing on the

areas that show considerable potential advantages as in the north coastal seas of both the United States and the U.K.

The availability of wave power, although immense, is found to be greater in certain coastal areas of the United States, just as solar and wind have high potential in some areas and not others. The Electric Power Research Institute estimates the wave resource of the United States to be 2,640 TWh/yr, or about 9 quads [21]. Figure 7 depicts the areas of near-shore potential wave energy for all the coastal United States that could reasonably be utilized. The densest areas for potential wave energy are along the Pacific coast of North America. The difficulty in capturing wave energy increases significantly as one ventures farther away from the coast, so although the resource may exist it may become prohibitively expensive given the current market.

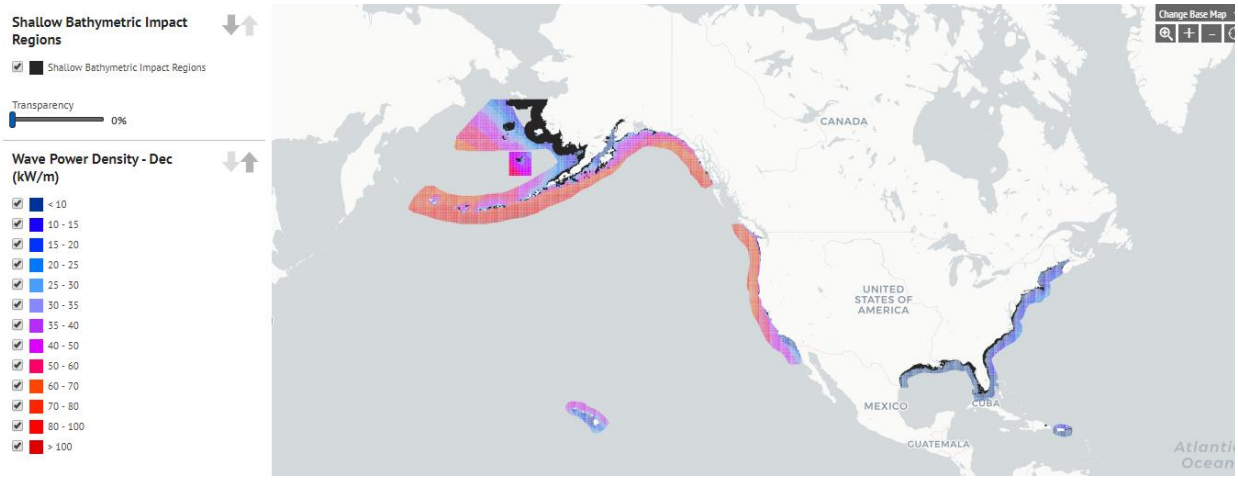

Figure 7. United States wave power resource [21]

Although the potential wave energy resource may not be as available to the entire continental United States as solar or wind, the potential benefits to coastal communities could be immense. The significant task of distribution and storage of energy for use across the country in all its different forms is

another topic entirely and should be examined further. Additionally, subjects such as energy return on investment (EROI) must be proposed for in depth analysis.

The above discussion has set the stage for studying and advancing the technology that will bring wave energy to fruition. Traditional non-renewable energy resources are being depleted, the environment has shown significant negative impact from the burning of fossil fuels and nuclear waste, and the wave energy resources are available but have yet to be a major player in the renewable energy supply.

Regardless of other factors – political, financial, and otherwise – the development of wave energy is still very much in its infancy and requires significant study to consider it as a future placeholder in America's energy portfolio.

1.9 Wave energy converters

The idea of capturing the potential energy of waves is called wave energy conversion and the device that accomplishes this is appropriately called a wave energy converter, or WEC. To harness power from the waves, there are different methods currently available. According to researchers Charlier and Justus, there are three basic ways to capture wave energy: "(1) the vertical rise and fall of waves to build up air or water pressure to run a turbine; (2) the wave caused rolling, pitching or heaving of a floating body, to run the turbine by means of cams or vanes; and (3) the focusing of waves into a converging channel creating thus the pressure to run the turbine" [4].

Based on the different ways in which the energy is captured, Falcao proposed the classification of the conversion devices described above into three major categories [15]. Figure 8 shows the breakdown and the further divisions for WEC devices.

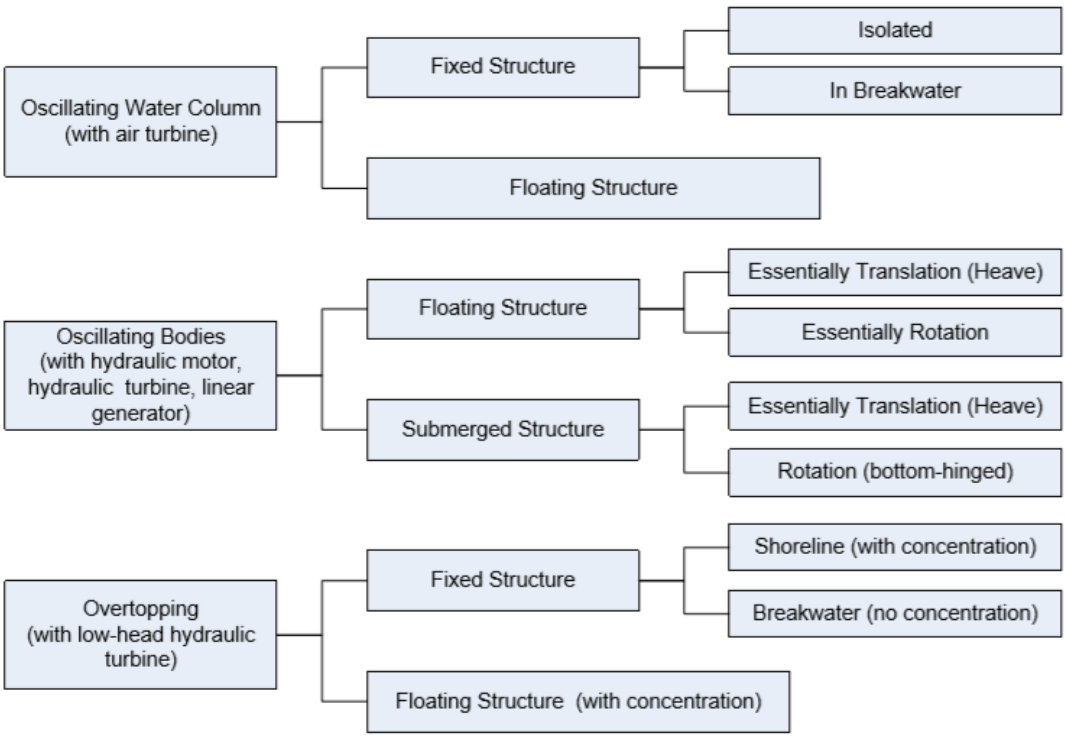

Figure 8. Classification of wave energy devices [15]

The first method of wave energy capture is through devices called Oscillating Water Columns (OWCs). OWCs use the wave motion to create a pressure differential against a fixed reference to push air or water across a turbine. These devices have shown good promise in both on-shore and off-shore applications, but mostly in rocky shores such as the Pacific Northwest and New England coastlines. There are also overtopping devices, which focus the incident wave to a reservoir and then utilize the height difference to employ the tenets of hydroelectric power generation. Both of these types have shown promise and are continually being researched and developed, however, the focus of this thesis is on a third type of WEC which will be discussed further.

In Charlier and Justus' description, the second method describes a WEC that oscillates due to the motion of a wave and then transfers the kinetic energy of the oscillating body through various means to mechanical energy then electricity generation [4]. The motion of waves can be broken down into six degrees of freedom, or modes of motion, and different WECs take advantage of these different modes of

motion. The six modes can be subdivided into rotational motion: roll, yaw, and pitch, and translational motion: heave, surge, and sway. These motions define the effect of waves on a floating body as seen in Figure 9.

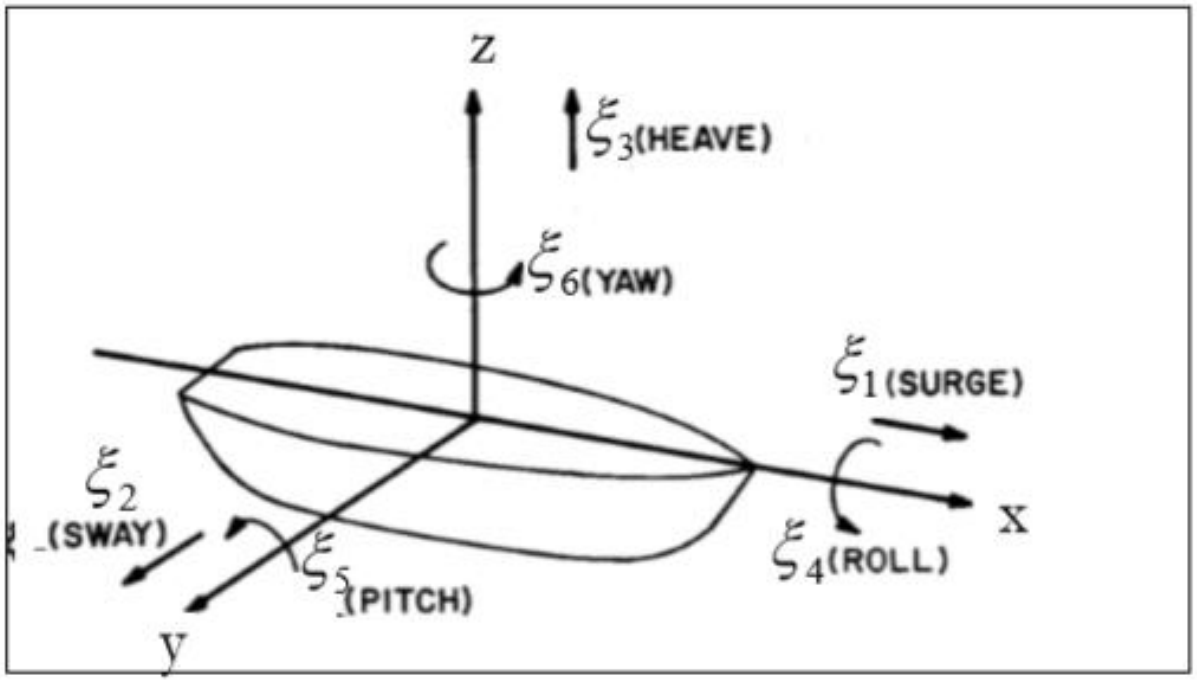

Figure 9. Six modes of motion for a floating body [11]

This information is important because the mode of motion is used to determine the mechanism by which the WEC will convert the energy into power and how to set up the formulas for solving the governing equations. Nearly all oscillating WECs rely on translational motion to provide the displacement for power capture, specifically, heave motion has shown to be exceedingly promising [7].

Another factor that affects the type of WEC employed is the device location relative to the shoreline. There are three areas where a WEC can be used: onshore, nearshore, and offshore. Each location has its advantages and disadvantages. An onshore device is less costly when it comes to deployment,

maintenance, and transmission costs, but may be unsightly and not have as much potential as deep water. A nearshore device, that is, a device that is deployed between 10-50m of water depth, is moderately easy to access but can only capture power from smaller waves. Additionally, many nearshore devices could potentially disrupt commercial industries and ports of entry. Offshore, or deep-water deployments of WECs benefit from the largest amount of wave potential but are also more costly and difficult to maintain. There is also higher risk for severe weather out in the open ocean.

Because of all the different variables involved in ocean waves: modes of motion, location, frequency, and amplitude, there have been thousands of patents issued for different ways to capture this great potential. In fact, the first patent, according to multiple sources, dates to 1799. Despite mainstream resistance or a lack of government incentive, there is encouraging development of these devices in countries like the U.K., France, China, Japan, Norway, the United States, and others. According to the website openwaveenergy.org, home of the Open Wave Energy Project, there are over 140 companies and Universities around the globe that have some level of involvement in wave energy conversion.

Some of the ideas for WECs are very innovative, but most fall within a few general categories. There are point absorbers (PA) which are defined as having a capture width significantly shorter than the wavelength of the incident wave and act primarily in heave motion. There are also attenuators, which are longer and run coincident with the incident wave, but also rely on heave in deep water. Point absorbers and attenuators both fall into the category of oscillating bodies under heaving motion according to the International Tank Towing Conference. Devices that take advantage of surge motion are called flap-type devices and are typically bottom fixed nearshore devices. Examples are shown in Figure 10.

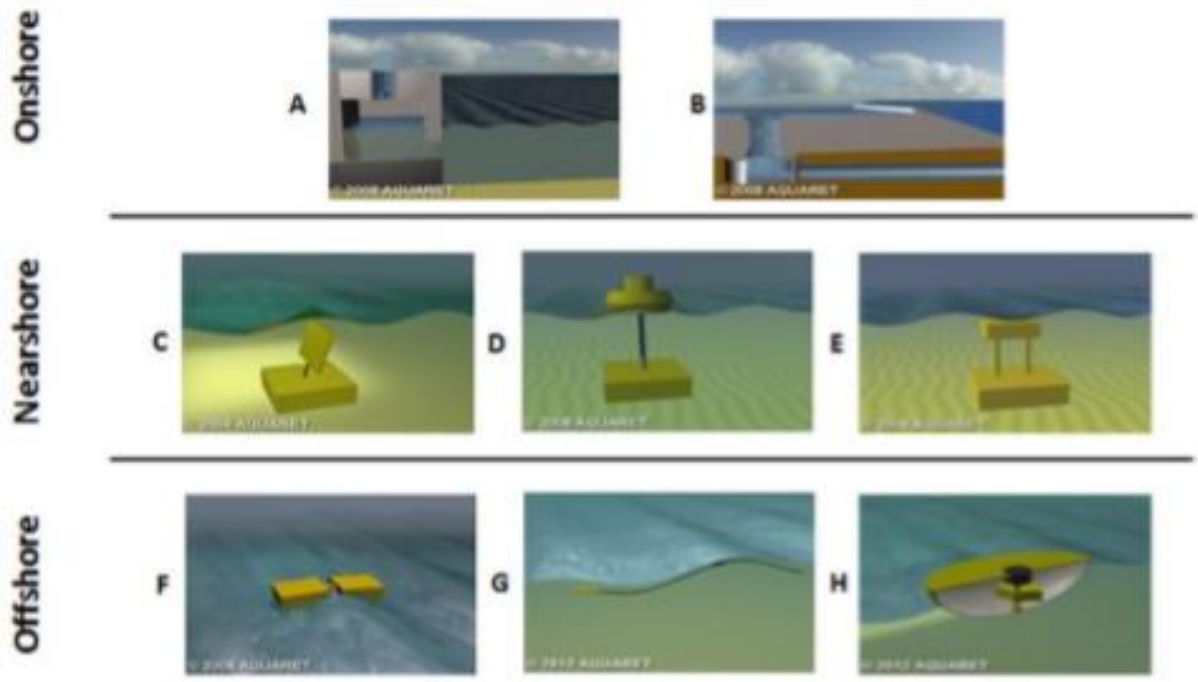

Figure 10. Examples of wave energy converters and device locations [48]

Wave energy converter is the name associated with these energy producing devices. However, the WEC is actually part of a larger system that has been dubbed the Wave-to-Wire system, or W2W. The W2W system is comprised of all the elements that take the power stored in waves through to electrical output. The different components of the W2W system are seen here in Figure 11.

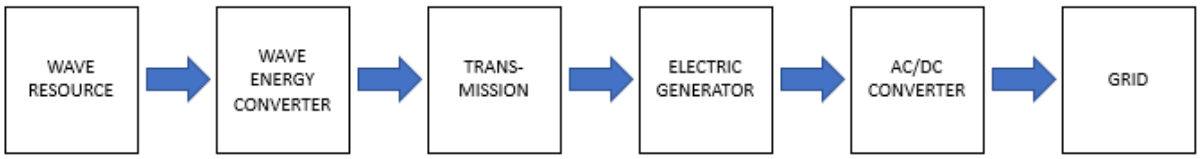

Figure 11. The wave-to-wire model [28]

Each of the components of this system are equally critical to the end state of producing electricity. The WEC is the first component of the system and is placed in the direct path of the waves. The second component is the transmission system. The purpose of the transmission system is to respond to the translational (or rotational) displacement of the WEC by applying a fixed or variable damping resistance that can be optimized to the device and the wave conditions. This in turn provides an equal and opposite mechanical force that drives the electrical generation system, such as the mechanical rotation of a generator's rotor. One type of a transmission system in the W2W model is the hydraulic Power Take-Off (PTO) system. As an example, a WEC moving up and down from wave action might cause a piston to move up and down, pressurizing a hydraulic transmission system. The PTO would then be used to drive a generator shaft. According to Penalba "hydraulic PTO transmission systems appear to be the choice of the vast majority of developers" [28]. Additional methods include pneumatic or mechanical transmissions, each with its own benefits.

The third stage of the W2W system is the electricity generation. The development of this technology has proved particularly challenging in the wave energy field specifically because of the very slow movement of the water compared to that of wind turbines. Although the energy content in the waves is high, the slow speeds are difficult to translate into rotational motion to drive electrical generation. There are several methods currently in use and under development to include the use of a hydraulic motor that is driven from multiple accumulators and then geared to spin the electric rotor. This can be easily mated to a hydraulic PTO system for simplicity of design. Another option that combines this stage and the PTO stage is a linear electric generator which can be effective but requires optimization of the displacement of the WEC.

The last stage before transmission to the grid is the conversion stage in which the determination is made for how to convert the mechanical motion into electrical potential. The conversion stage has been thoroughly studied in numerous other fields and although it remains a critical component of the W2W system, it does not appear often as a topic in WEC research. Any device being installed in the ocean will

be subject to the harsh ocean environment. This includes the elements of seawater and its deleterious corrosive effects, biofouling, and violent storm conditions. WECs are not different. It creates a unique and substantial technological challenge that cannot be ignored in design.

Through studying all the various research, patents, and conferences, it becomes clear that as a field of study, wave energy conversion is very broad and not one device has captured the attention of investors or governments. It's safe to say that when discussing solar and wind technologies there are a few go-to options that have been proven over the last few decades. With WECs, that is just not the case.

1.10 Design of experiment and hypothesis

This research attempts to approach the design process for WECs from an engineering optimization perspective in the hopes that a fundamental design can be achieved. To do so, a partially submerged buoy point absorber type WEC has been selected that is intended to be deployed nearshore in water depths of around 50m. The selection of this type of device is based on its simplicity, deployability, scalability for use in multiple buoy arrays, and flexibility for use in multiple scenarios.

A surface floating buoy point absorber has different properties that affect the power production. It is the goal to select the best combination of properties for a given installation location to achieve the best performance, which is denoted as optimization. For example, recent work has been conducted on the optimization of point absorber buoys, regarding buoy draft and diameter [33]. Other works include optimization of two dimensional shapes using diffraction and linear wave theory [11]. The different performance of submerged versus floating buoys has been explored and computational fluid dynamics (CFD) has been applied to spherical buoy WECs. Through iterative optimization and CFD, this experiment attempts to determine an optimized buoy geometry that can be applied to a WEC independent of other factors like diameter and draft.

If a buoy shape for a point absorber WEC can be determined through optimization to show a 10% or higher improvement in absorbed power over other shapes at multiple drafts, diameters, and sea states, then the further development of WECs with that resultant buoy shape should emerge as an appropriate building block for further development of Wave Energy Converters.

CHAPTER 2

LITERATURE REVIEW

2.1 Maximum energy capture from floating bodies

In the last half century, the study of how to extract useful power from water waves has increasingly become a focus for researchers worldwide. Pioneers such as Falnes, Budal, Masuda, Mei, and Salter have thoroughly developed the fundamentals of wave energy extraction and the behavior of oscillating bodies in water waves. In the foundational book, "Ocean Waves and Oscillating Systems" Johannes Falnes derived many of the mathematical formulas required to understand the characteristics of water waves and the interaction with floating bodies [7]. Specifically, he examined the buoy type point absorber wave energy converter in heave motion. He explains that, "for any given wave, the maximum energy that can be absorbed by a heaving axisymmetric body [e.g. point absorber WEC], equals the wave energy transported by the incident wave front of equal width to the wavelength, λ, divided by 2π" [7]. This is an extremely useful relationship and will be discussed in detail because that serves as an upper bound for all possible designs of WECs that are axisymmetric.

The performance of a PA type of WEC depends upon the physical properties of the ocean, the geometry of the passing waves, the resulting forces on the device due to the wave excitation forces, and the resulting motion of the device. A review of each of these topics and relevant governing equations follows.

2.2 Fluid dynamics properties

To better understand what exactly Falnes was describing, an outline of the characteristics of water waves is required. The principles of fluid dynamics are applied in all WEC design and optimization, so a brief review is warranted. In scientific study, the base properties of water are measured at 4°C. Density and specific weight are often referenced in fluids problems and have the values shown below.

Specific weight	$\gamma_w @ 4℃ = {}^{9.81kN}/_{m^3}$
Density	$\rho_w @ 4℃ = 1000\,{}^{kg}/_{m^3}$

Additionally, the hydrostatic pressure that exists in water can be expressed as a function of the specific weight of the water multiplied by the depth as measured from the surface of the water, that is:

$$\Delta p = \gamma h \qquad [1]$$

2.3 Wave geometry and linear wave theory

Some of the basic components of a regular waves are depicted in Figure 12. The wavelength is measured from peak to peak, and the wave period is a measure of how many seconds it takes between the crossing of two subsequent wave peaks across a single point of reference.

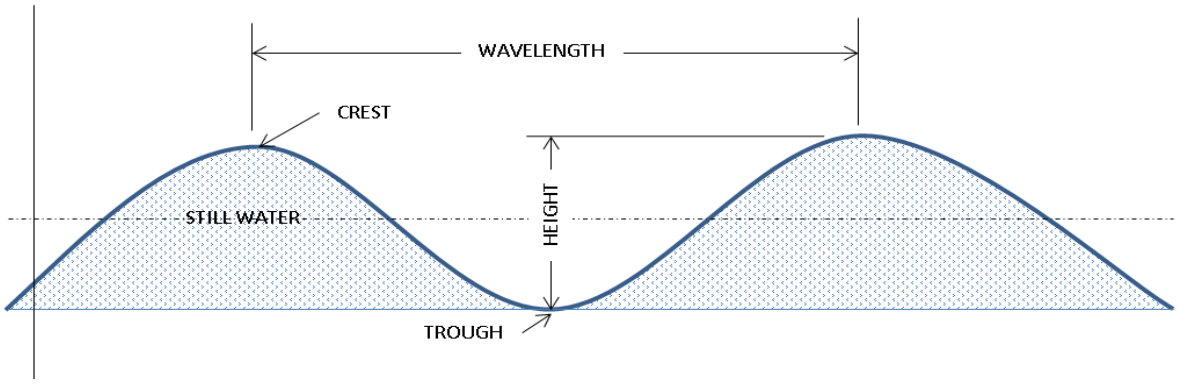

Figure 12. Regular wave components

The wavelength and period of waves may be expressed in terms of the water depth, acceleration of gravity, etc. In order to develop these relationships, some fundamental assumptions must be made. According to Krogstad and Arntsen, the water is assumed to be incompressible and irrotational, and in accordance with the principles developed in basic fluid dynamics, Laplace's equation must be satisfied for any water particle in terms of its velocity potential, ϕ, away from the boundaries and the free surface [17]. That is:

$$\frac{\delta^2\phi(x,z,t)}{\delta x^2}+\frac{\delta^2\phi(x,z,t)}{\delta z^2}=0 \qquad [2]$$

where *x* and *z* are the coordinates of the water particle using a standard global coordinates axis (*z* direction pointing upwards, perpendicular to the free surface). In an ideal example, it is assumed that the water is in an open flow channel with a regular bottom, and the bottom of the channel is assumed to be impermeable to water. Therefore, the velocity at the bottom must be zero at all times, and so the velocity potential at bottom surface boundary condition must satisfy:

$$\frac{\delta\phi}{\delta z}(x,z=-h,t)=0 \qquad [3]$$

where -*h* is the distance below the free surface in the negative *z* direction, i.e. the bottom of the channel. Assuming an ideal fluid and regular waves that are not breaking, a fluid particle at the surface should remain at the surface at all times, and so the velocity of the particle in the *x* and *z* planes can be related to the surface elevation, η. This is called the kinematic boundary condition, where *u* and *w* are the velocity of the particle in the *x* and *z* direction, respectively, and is expressed

$$\frac{\delta\eta}{\delta t} + u\frac{\delta\eta}{\delta x} = w \quad [4]$$

Lastly, the pressure at the free surface is equal to the atmospheric pressure, derived from Bernoulli's equation, this is called the dynamic boundary condition:

$$\frac{\delta\phi}{\delta t} + \frac{1}{2}(u^2 + w^2) + g\eta = 0 \quad [5]$$

The water particle must satisfy Equations 2–5, which is a highly complex problem, and a solution is not yet known for it. To make it simpler, researchers and scientists have determined that the problem can be linearized thus making calculations much more manageable. Dimensional analysis and scaling are used to linearize the equations and boundary conditions and requires the assumption of small amplitude waves, that is, the amplitude is much smaller than the wavelength, $a << \lambda$ [17]. This is referred to as Linear Wave Theory (LWT). There are other types of waves such as Stokes and cnoidal, but the analysis becomes much more complex. As defined by Le Méhauté, linear wave theory is applicable to deep water waves according to Figure 13 [19]. Deep water is defined as having a depth at least 1/3 to 1/2 of the wavelength.

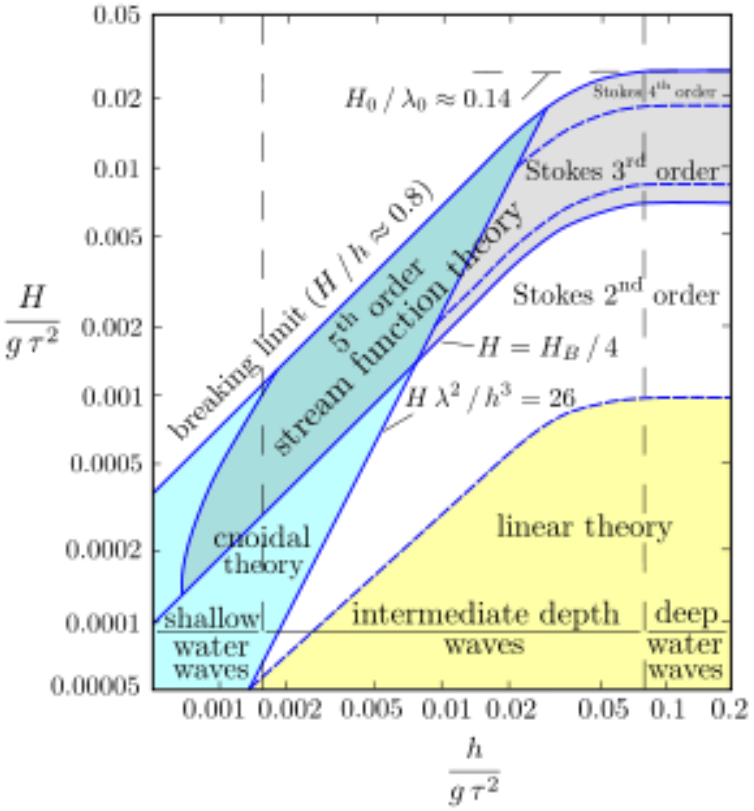

Figure 13. Applications of linear wave theory [19]

2.4 Application of hydrodynamic diffraction

Linearization produces an invaluable set of relationships and characteristics that are utilized in the WEC field in the process known as hydrodynamic diffraction. A summary of these relationships can be found in appendix A [17]. It has further been extensively studied that LWT can be used to sufficiently approximate the hydrodynamic parameters of a floating body oscillating in heave. One of these parameters is the Froude-Krylov force, which can approximate the excitation force. This is defined by Falnes as, "fixed, a non-vanishing potential φ is the result of an incident wave, only. In such a case F_j is called the "excitation force" [7]. The excitation force can be approximated by the Froude-Krylov force by neglecting the incident wave, which can hold reasonably true for a buoy of which "the extension of the buoy is very small compared with the wavelength." [7]. Falnes derives the excitation force as:

$$F_{e,j} = i\omega\rho \iint_S (\hat{\varphi}_o + \hat{\varphi}_d) n_j dS \quad [6]$$

which means that the force acting on the body in the heave direction can be computed based on the integration of the velocity potential multiplied by the normal force over the wetted surface of the submerged body. The approximation of this force can be solved using commercially available software such as Aqwa from ANSYS.

LWT is appropriate for use when examining small amplitude waves in deep water. However, as wave amplitude increases the results that are obtained using LWT become less relevant and accurate power estimates have been pursued in research using non-linear theory in more complex, realistic sea states, and can be modeled in Computational Fluid Dynamics (CFD) modeling software. However, according to Palm, "computational costs for VOF-RANS [non-linear modeling] are orders of magnitude higher than linear radiation-diffraction methods" [26]. Because of the nature of this study and the deterministic factors being more relative rather than quantitative, LWT is used to approximate the power output of the WECs being studied. Other studies have shown good agreement with experimental results using LWT.

2.5 Relevant studies using linear wave theory

Using LWT Linnea Sjökvist calculated the numeric response for a PA type WEC and compared it to experimental results with good agreement in small amplitude waves as seen in Figure 14 [33]. For the experiment, the hydrodynamic parameters were found using the software COMSOL Multiphysics, using a Finite Element Method approach, and WAMIT, using the Boundary Integral Element Method (BIEM). The results were then used to input into the equations of motion for the WEC (which will be discussed later) to solve for the power capture of the devices.

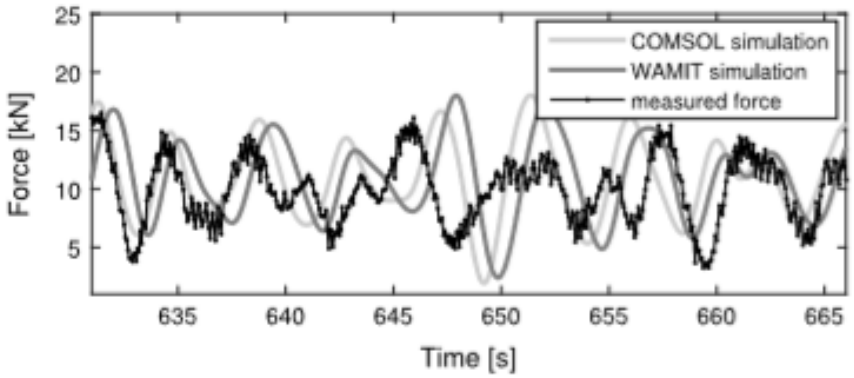

Figure 14. LWT compared to experimental results [33]

Penalba considered not just the buoy geometry for a floating point absorber, but also the effects of placing multiple buoys into an array to make a wave energy farm capable of producing higher power [29]. The notion of creating a wave energy farm has been presented many times because of the economy of scale that can be applied, reducing the overall LCOE for wave power and is the most likely employment of WECs in the future. By deploying a number of different diameter buoys, one can take advantage of achieving resonance in varying sea states. In the study, the research also uses diffraction theory, based on LWT to determine the hydrodynamic parameters of the devices using Aqwa. Those results are then used to calculate absorbed power for each configuration. It is also shown that placing devices in close proximity results in destructive interference, reducing power output.

An optimization study is one that observes the characteristics of a device, how these characteristics affect the outcome and ultimately determine what options provide the best efficiency for a given scenario. For the PA, the geometry is to be optimized that reduces negative hydrodynamic characteristics, exploits the positive ones, and gives the most power. Given the large number of variables to consider, this is most easily done using computer software. Computer modeling prior to real-world testing provides valuable input and saves time and money. Several researchers have conducted optimization experiments on PA buoys previously using both computational models and experimental studies.

Hager utilized the radiation-diffraction method and Aqwa to determine the hydrodynamic parameters on PA type buoy WECs of varying geometry in two dimensions to examine in more detail the effects of buoy design on overall power efficiency [11]. To do so, she created 39 different models in a 3D modeling software and ran numerical simulations to determine the complex amplitude of the excitation force then derived an equation to determine the overall efficiency of the device. The results showed that as the geometry became more convex, that is, approaching hemispherical, the efficiency is much better than for that of the buoy as a cone shape and even more so for a teardrop, or more concave shape. However, the excitation forces on the concave bodies were higher than for that of the hemispherical buoys, when measured as the incident wave hits the curved surface. The uniqueness of this experiment is that the buoy is not axisymmetric and so a special formulation for efficiency is derived and cannot be applied to an axisymmetric buoy but does show the capability of parameter optimization using Aqua and manually altering the geometry.

A study conducted by Pastor and Liu takes a similar approach but for a 3D model. In that study, the effect of the bottom shape was examined, using two distinct shapes, a hemispherical bottom and a conical bottom with an apex of 120°. Additionally, three different radii were proposed and tested [27]. Similar to the Hager study, the conical buoy produced higher excitation forces than the hemispherical buoy, but conversely, the conical buoy showed a slightly higher power absorption than the hemispherical at what was chosen as the optimum diameter and draft of 3.5m and 2m, respectively. This shows the potential differences in using a 3D axisymmetric model versus a 2D model and requires further refinement to combine the best of both approaches.

The hydrodynamics of a PA buoy as ocean water flows in and around it will affect the power absorption. For example, there may be two buoys that have the same wave force induced but one may have better hydrodynamic characteristics and hence be more efficient. Poor hydrodynamic characteristics cause drag, frictional losses, and vortices. It was shown experimentally by Zang that vortices form on the edges of a flat bottom cylindrical heaving buoy which could introduce viscous losses into the system. The

experiment found that the "total damping of a floater with a flat bottom can be larger than a modified shape by up to 67%" [50]. The vortex shedding can be seen in Figure 15.

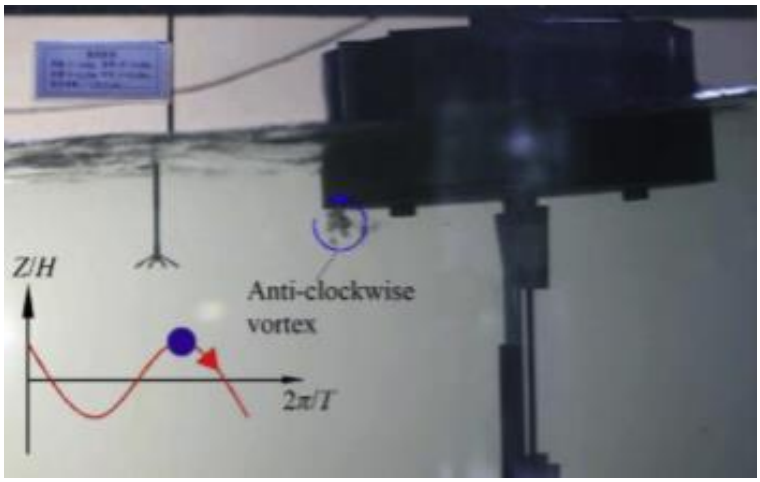

Figure 15. Vortex shedding on flat-bottom buoy [50]

One method to optimize buoy geometry using a software platform regarding diameter and draft for a device is presented by Shadman, in which the upper and lower bounds of the buoy diameter are established using the fundamentals from Falnes, and the draft is optimized to match the buoy heave natural frequency to the prevailing sea wave frequencies [32]. This was done by first determining the maximum possible capture width based on the wavelength for the predominant sea states, using the formula from Falnes, "Ocean Waves and Oscillating Systems" [7]. The maximum possible absorption width, L_{max} is

$$L_{max} = \frac{\lambda}{2\pi} \quad [7]$$

Furthermore, according to Shadman, the capture width ratio for successful devices should satisfy the relationship:

$$C_{wr} = \frac{L_{max}}{D} \geq 3 \quad [8]$$

where D is the buoy diameter of the device. This expression provides an empirical formula for initial sizing of a PA. Alternately, Falnes recommends that buoy diameter should be between 5-10% of the incident prevailing wavelength. These bounds are developed utilizing the characteristics of deep water waves and LWT as previously described, relating wavelength to period [7].

Shadman then establishes the optimum draft using the theory that the optimum power is developed when the heave resonance of the buoy matches the frequencies of the prevailing sea states. He determined the required added mass needed to bring the buoy to resonance by showing natural frequency as a function of cross sectional area at the free surface of the water A_{wp}, the mass of the buoy m_b (based on the selected diameter and draft), and the required added mass m_a, shown here in Equation 9.

$$\omega_n = \sqrt{\frac{\rho g A_{wp}}{m_b + m_a}} \quad [9]$$

It is important to remember at this juncture that true optimization of point absorber WECs can only occur for specific sea state characteristics. That is, as the period of the wave changes, the buoy no longer achieves resonance, and therefore does not produce the maximum amount of power. To that end, additional research is being conducted to optimize PTO damping and added mass using various techniques that can allow for the buoy to achieve resonance at different wavelengths. Phen See presents an optimization of an all-electric PTO using a method called Ant Colony Optimization, a bio-inspired algorithm that provides fast real-time ability to achieve resonance in irregular waves [30]. This is a CRITICAL portion of WEC development and should be addressed in the W2W whole systems approach. For the purposes of this

experiment though, damping and added mass is optimized for a specific sea state in order to focus on the impacts of changing the geometry of the wetted surface of the buoy. The assumption made here is that a geometry that performs the best when the PTO damping and added mass is optimized will also perform the best when that is not the case.

Shadman continues by using the results of the hydrodynamic parameters as solved in Aqwa. A few different combinations are tested at a range of frequencies and optimized using a software called Minitab. The measures of performance in the study were not just peak power, but also which shape combinations (diameter and draft) produced the most power over the largest range of frequencies. This study is an excellent work into the effects of diameter and draft on overall power performance. However, the buoy studied was a regular cylinder so does not take into account different geometry of the wetted surface. Regardless, for the variable sea states chosen based off the hindcast data for the Rio de Janiero region, the optimal diameter and draft for the study was 13.5-m diameter, and 5-m draft. Interestingly, the changing draft appeared to have more significant effect on the overall power absorption.

For the studies referenced thus far, the aim was to determine the hydrodynamic parameters of the device to include added mass, radiation damping, and excitation force. The next step was to compare and contrast the results using some metric defined by the researchers that could be universally applied. Stansby utilizes the metric of effective capture width ratio as a basis for comparison of various heaving buoys [36]. Other research has looked at time-averaged power, resonance bandwidth, and peak power.

2.6 Measures of performance

According to Sokolowski and Banks, when developing any experiment to investigate a system, the outcomes, known as measures of performance, must be identified. For all experiments, the measures of performance must be quantifiable, accessible, and measurable, aligned with the goals of the experiment, and meaningful [35]. As previously described, in the energy industry the most significant measure of

performance gets right at the bottom line, the Levelized Cost of Electricity. However, the broad discussion that ensues from studying in detail costs such as transportation, storage, and myriad other factors is beyond the scope of this paper.

A better measure of performance in this case will be simply the power output of the device as measured in either the frequency or time domain. The challenge of this is to determine how exactly to measure the power. A good starting point is to define what is already known about the upper bounds of the possible power production capabilities. This has been studied at length by Falnes and others and is referenced in nearly every discussion of WECs. Falnes derives the maximum energy flux per unit wave crest width that can be absorbed by a buoy in heave using the peak period, T_p, and the significant wave height, H_s, such that:

$$J = \rho g^2 T_p {H_s}^2 / 32\pi \qquad [10]$$

where the peak period is defined as the wave period with the highest amount of energy according to the spectral frequency as determined using the JONSWAP or Pierson-Moskowitz wave spectral density functions [7]. The JONSWAP was a joint scientific venture which resulted in an empirical structure of the source function of waves in the North Sea and is used as a standard in many wave energy projects [14]. Because of the variability of irregular waves, the spectral density function is an invaluable tool used to determine wave characteristics which have been developed using historical wave data. The significant wave height is defined by the National Weather Service as, “the average of the highest one-third (33%) of waves (measured from trough to crest) that occur in a given period” [25].

For example, using a sea state which has a significant wave height of 1m and a peak period of 8s as inputs into equation 10, an energy flux of 7.64kW/m is calculated. Falnes further describes the maximum power absorption using the maximum capture width from Equation 8 which results in:

$$P_{max} = JL_{max} \quad [11]$$

In this example, with a period of 8s, the wavelength is calculated as approximately 100m, having a maximum absorption width of 15.9m, and a maximum possible power of 121 kW. That is the maximum theoretical power which can be absorbed by an axisymmetric body in heave for those wave conditions.

Using the rule that the diameter of the buoy should be related to the maximum capture width and wavelength as described in Equations 8 and 9, the optimum diameter for a buoy in this case is 5.3m. This formula serves as a reference point for estimating the efficiency of PA WEC operating in heave only for small amplitude waves, using LWT.

2.7 Governing equations

In order to numerically solve for the power capture of a WEC in heave motion only, the forces acting on the body must be solved for using Newton's second law and the conservation of mass and momentum. The coordinate system for this analysis is a global system in which *x* represents the direction of travel of a wave, *y* represents the width across which the wave exists, that is, perpendicular to the direction of travel, and *z* represents the positive direction upwards from the water surface. When you examine the static forces on a floating body, you have the weight of the buoy acting in the negative *z* direction (towards Earth) and the hydrostatic pressure, or buoyancy force acting upwards. With no external forces these opposing forces are equal and the buoy is at rest. The buoyancy force, F_b, is defined by the volume of the fluid displaced, and the density of the fluid, in this case water. Written out you have:

$$F_b = \gamma_f V_d \quad [12]$$

If a mooring line is then introduced with a given axial stiffness, the buoy will be anchored to the seabed. The mooring line can be represented in a model by a spring force with a constant coefficient. Additionally, the buoyancy force, which changes with volume of displaced fluid as the buoy oscillates, is represented by a hydraulic damping coefficient which is dependent on the geometry of the floating body. The resultant system resembles a spring-mass damper system as shown in Figure 16.

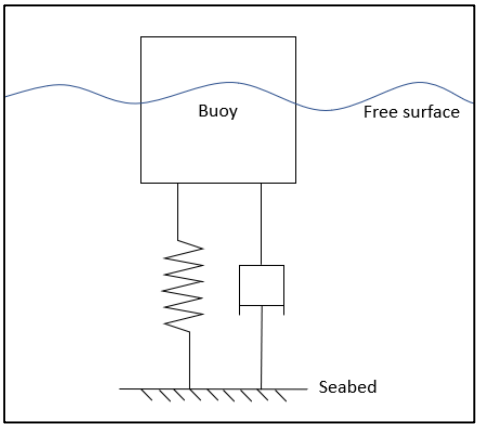

Figure 16. Heaving buoy static equilibrium model

The static equilibrium equation with no external forces for a spring mass damper system dictates that the sum of the forces acting on the body are zero. That is:

$$\sum F_z = 0 = ma + bv + cx \qquad [13]$$

where m is the mass of the buoy, b is the damping or hydrostatic restoring force coefficient, c is the hydrostatic stiffness coefficient, and a, v, and x are acceleration, velocity, and position of the buoy, respectively. Alternatively, it is useful to express the acceleration and velocity in terms of the position using the first and second derivative with respect to time, thus:

$$m\frac{d^2z(t)}{dt^2} + b\frac{dz(t)}{dt} + cz(t) = 0 \quad [14]$$

where *z* replaces *x* as the term representing the position of the buoy in heave as is common practice for hydrodynamic analysis of floating bodies. This is a linear second order, homogenous, differential equation with the known solution:

$$z(t) = (C_1 cos\omega_d t + C_2 sin\omega_d t)e^{-\delta t} \quad [15]$$

When a body is impinged upon by a wave in the ocean, an external force is added to the equation, such that,

$$m\frac{d^2z(t)}{dt^2} + b\frac{dz(t)}{dt} + cz(t) = f(t) \quad [16]$$

In the hydrodynamic analysis of floating bodies, additional forces that affect the oscillating body can also be included in the equation and the coefficients of each term must be determined in order to solve the equation. That is, the addition of mass, fluctuation of the axial stiffness, changing of the buoyancy force through different diameters and geometric shapes, and the introduction of an outside force all affect the solution to the position of the buoy in the frequency and time domain. The other external force that is added in the case of a wave energy converter is the PTO force, as previously mentioned, which serves as the power capture device. Other forces that should be considered include friction and viscous forces. In this example, however, those forces are set aside because they are not considered when using linear wave theory. In further stages of WEC development, they should be considered for more complete accuracy in power

estimates. The full governing equation for the motion of the oscillating body in the time domain for this experimental setup is written:

$$\left(m_b + m_a + m_{sup}\right)\frac{d^2z(t)}{dt^2} + \left(b_{ext} + b_{hyd}\right)\frac{dz(t)}{dt} + cz(t) = f_e(t) \quad [17]$$

where m_b represents the mass of the buoy, m_a is the added mass (calculated in Aqwa), and m_{sup} is the supplemental mass that can be adjusted by the user. b_{ext} is the radiation damping coefficient of the external PTO that is determined later, and b_{hyd} is the radiation damping coefficient of the oscillating body (also solved in Aqwa). The last term, f_e, is the excitation force described previously which is the force exerted by the incident wave which causes the oscillation of the body. This force is frequency dependent, as is the radiation damping and added mass. These parameters depend on the geometry of the body and the sea state. Each time the sea state changes or the buoy changes, the position and velocity change accordingly. Converting from the time domain to the frequency domain using a Laplace transform, the equation becomes

$$\left(m_b + m_a(\omega) + m_{sup}\right)\omega^2 Z + \left(b_{ext} + b_{hyd}(\omega)\right)\omega Z + cZ = F_e(\omega) \quad [18]$$

Then combining Equation 18 with Equation 6 and including the definition of velocity potential given for LWT in deep water from Appendix A, the result is Equation 19.

$$\left(m_b + m_a(\omega) + m_{sup}\right)\omega^2 Z + \left(b_{ext} + b_{hyd}(\omega)\right)\omega Z + cZ = i\omega\rho \iint_S \left(\frac{ag}{\omega} e^{kz}\cos(\omega t - kx)\right) n_j dS \quad [19]$$

where a is the wave amplitude, g is the acceleration of gravity, and k, also called the wave number, is $\frac{2\pi}{\lambda}$. In regular waves the wave amplitude is fixed. However, in irregular waves, the wave amplitude is described in terms of the JONSWAP wave spectrum which is written:

$$S_j(\omega) = \left(\frac{ag^2}{\omega^5}\right)^{\left[-\frac{5}{4}\left(\frac{\omega_p}{\omega}\right)^4\right]} * \gamma^{\left[-\frac{(\omega-\omega_p)^2}{2\sigma^2\omega_p{}^2}\right]} \quad [20]$$

2.8 Computational analysis and solving for power extraction

The Aqwa solver combines the linearization of the governing equations of motion of water particles and the forces acting on an oscillating body and determines the excitation force, added mass, and radiation damping in the Hydrodynamic Diffraction analysis system of ANSYS 19.1. Using these inputs, a hydrodynamic response can be found given a sea state using regular or irregular waves. When an external PTO is simulated through the insertion of an additional hydraulic damping force, a power output can be determined. As reported by Gaunche [9], when the PTO force is introduced into the system, the mean absorbed power can be calculated using the formula:

$$\bar{P}_{absorbed} = \frac{\int_{t_1}^{t_2} F_{GEN} \times \frac{dz(t)}{dt} dt}{t_2 - t_1} \quad [21]$$

where

$$F_{GEN} = b_{ext} \times \frac{dz(t)}{dt} \quad [22]$$

These formulas can then be used numerically and experimentally to calculate the power of the WEC for different geometries. In the Hydrodynamic Response solution of the Aqwa solver, the instantaneous velocity of the heaving body is found at each time step, and then, combining Equations 21 and 22, the instantaneous power of the WEC can be determined as well as the time-averaged power. The ability to extract power from a wave energy converter is not as simple as adding a PTO however. By introducing a new force into Equation 19, the oscillation of the buoy is impacted and therefore the velocity changes as well. In the next section, the method describes how the model and simulation were set up in order to determine the overall impacts of the geometry of the buoy on the power capture ability.

CHAPTER 3

METHOD

3.1 Model development and analysis set-up

It has been shown that the hydrodynamic properties of a floating body can be calculated using the commercial software ANSYS Aqwa for different sea states. These properties include the excitation force (approximated from the Froude-Krylov force), the radiation damping coefficient, and the added mass. With these, the theoretical power capacity of different types of buoys can be compared based on changes in the geometry of the bottom surface. Initial set up of the Aqwa solver includes defining the sea states to include the density of water, gravity, depth, wave period, and direction of wave propagation.

In this experiment the density of water at 4℃ is defined as 1000kg/m^3. The water depth is set to 50m in accordance with the LWT application [7]. The length and width of the numerical wave tank (NWT) are sufficiently large to prevent any destructive interference. Four different shapes of buoys are considered in this study that represent a wide range of shapes for an axisymmetric buoy as seen in Figure 17.

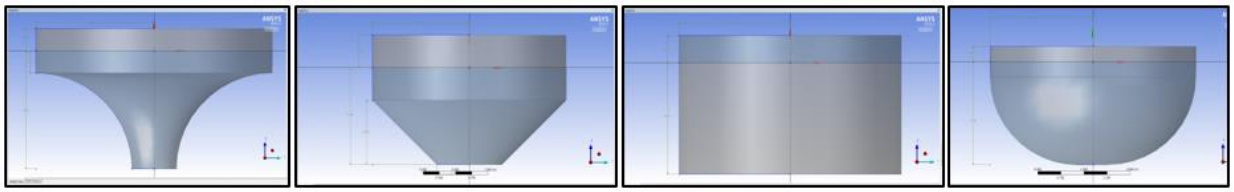

Figure 17. Four experimental shapes of axisymmetric buoys

As the figure depicts, each buoy is divided into 2 sections, the bottom of which represents the wetted surface of the buoy, the top of which would be the portion of the buoy that would be above the free surface of the ocean. The diameter of the buoys varies for each sea state that is tested in accordance with the previously described relationship between wavelength and maximum capture width. It is important to

remember that this is the purely theoretical value and the power capture ability of buoys in a real-world setting improves with increasing diameters to a certain point but that is not represented by the governing equations described. Further modeling using the VOF-RANS (Volume of Fluid-Reynold's Averaged Navier Stokes) method is recommended for those conditions. The values derived here serve as a fixed initial condition by which the effects of changing the geometry can be compared while still adhering to the formulations.

The next consideration in the design of the buoy is the draft and the height of the buoy above the waterline. These two dimensions are somewhat arbitrary but are important factors in the results of the experiment. When considering a floating body, especially in this case, it is critical that it be stable as it oscillates in the waves. Buoy stability, along with stability for any floating body, can be calculated based off the dimensions and center of gravity. The draft, or distance to the bottom of the buoy from the free surface, along with the height above the water will be determined by the density of the object and, in turn, the volume of the displaced fluid as the buoy sits in the water. Conversely, in an Aqwa simulation, the dimensions can be prescribed and then the solver will determine the mass of the buoy that produces that level of buoyancy.

Once the dimensions of the buoy are known, as well as the buoyancy force, a new term is defined called the metacenter, which is defined as "the intersection of the vertical axis of a body when in its equilibrium position and a vertical line through the new position of the center of buoyancy when the body is slightly rotated" [23]. A buoy will be stable if the center of gravity is below the metacenter, and the distance to the metacenter from the center of buoyancy is proportional to the least moment of inertia of the section of the body that intersects the free surface of the water, as shown in Figure 18.

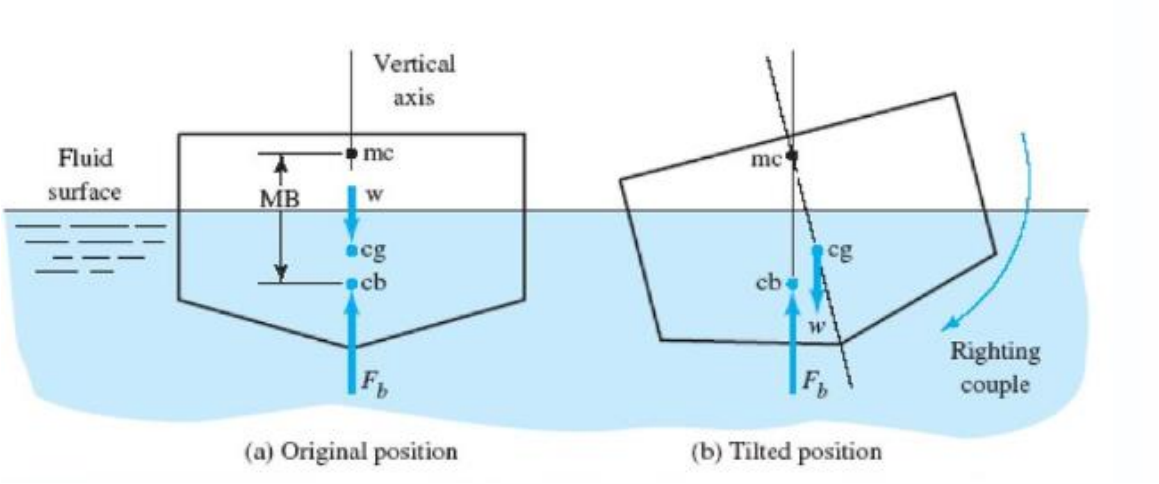

Figure 18. Method of determining buoy stability

Table 1 was developed to compute the stability of the cylindrical floating bodies selected for testing.

Table 1. Buoy Stability Calculations

Diameter (m)	**Height (m)**	**Distance above water line (m)**	**Distance Below waterline**	**CG measured from bottom**	**Center of Buoyancy**	**Moment of Inertia**	**Vol disp. Fluid (m^3)**	**MB**	**Y_{mc}**	**Stable**
2.98	1.99	0.50	1.49	0.99	0.74	3.87	10.38	0.37	1.12	TRUE
4.05	2.53	0.50	2.03	1.26	1.01	13.27	26.17	0.51	1.52	TRUE
5.30	3.15	0.50	2.65	1.57	1.32	38.61	58.32	0.66	1.99	TRUE
6.70	3.85	0.50	3.35	1.93	1.68	99.06	118.24	0.84	2.51	TRUE
8.27	4.64	0.50	4.14	2.32	2.07	230.12	222.48	1.03	3.10	TRUE
10.01	5.51	0.50	5.01	2.75	2.50	493.28	394.14	1.25	3.75	TRUE

An initial distance of 1m above the water line was chosen for the different diameters and it was determined through trial and error that at a height of 1m, the buoys of smaller diameter were not stable. Further trial and error found that 0.50m was a small enough value to produce stability in the smallest diameter buoy, and all the remaining buoys of larger diameter were also stable. Because of this, the same dimension was applied to all the buoys. A smaller value than this all the way to zero would also result in a

stable buoy, but the chosen value would ensure that the buoy would be visible to oncoming vessels as well as reduce the amount of overtopping of waves.

The draft of the device was chosen based on the diameter in such a way as to result in a practical overall design. As previously shown by Equation 9, the optimum design of a buoy's draft can be calculated by setting the natural frequency of a buoy in heave to the frequency of the incident wave, then solving for the draft, L, which is a function of the mass based on the displaced volume such that:

$$L = \frac{g}{\omega_h} \qquad [23]$$

where g is the acceleration of gravity and ω_h is the heave natural frequency, matched to the incident wave. This allows the designer some flexibility in the design of the buoy because a supplemental mass can be added to the buoy such that the natural frequency can be achieved without changing the draft. These values are also added into the equation of motion and used to calculate the position of the buoy.

The changing shape of the bottom of the buoy, which is the particular focus of this study, was based on the idea that the forces caused by the interference of the oscillating body with the wave might be impacted by the angle and curvature of the surface of the body. Stansby, et al. showed a 60% increase in power production of a rounded base buoy over a flat bottom shape [35]. Hager, Pastor, and Liu also showed improved performance with various shapes [11, 27]. To that end, the first buoy remained cylindrical to serve as a baseline for the experiment. The cylinder occupies the maximum volume possible for an axisymmetric body and has the most surface area accordingly. This fact should result in a higher overall excitation force because of the previously discussed integration of the velocity potential over the entire wetted surface. The draft of the buoy was equal to the height above the waterline plus the radius of the buoy. The buoy designs were constructed using ANSYS Design Modeler, the first of which is shown in Figure 19.

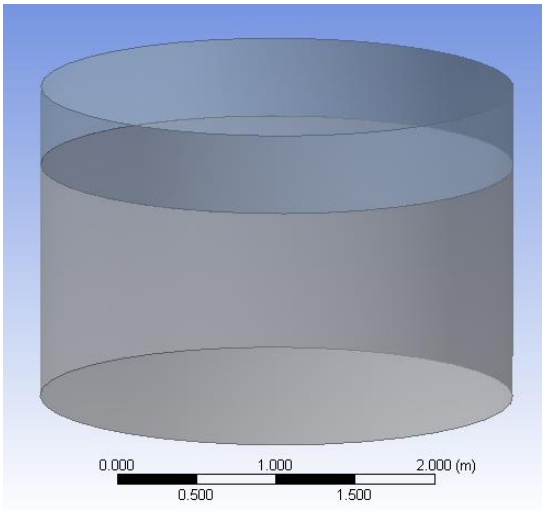

Figure 19. Cylindrical buoy

For the hemispherical shape, the radius of the arc was assigned as the radius of the buoy minus the distance above the waterline. This resulted in an area at the bottom of the buoy with a flat surface of 1-m diameter which could be used to attach an anchor point for a mooring line. This also ensured a 0.5-m portion of the buoy draft directly below the waterline was cylindrical. The rational for this is that parts of the buoy nearest to the free surface may encounter the situation where it is no longer in contact with the water due to the oscillation of the waves, and so to control the adverse effects on the buoy, each design looks the same down to 0.50m below the water's surface. The hemispherical buoy with a 4.05-m diameter is shown here in Figure 20.

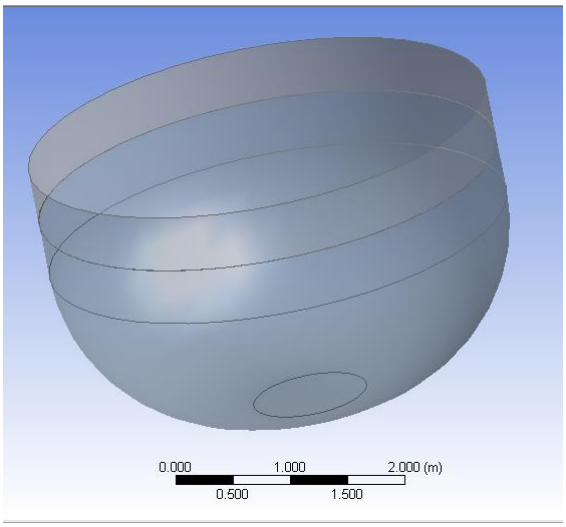

Figure 20. Hemispherical buoy

The conical buoy maintained the same constants as the other buoys in terms of intersecting area of the free surface, and the shape variation was created by defining a chamfer at a 45° angle to the vertical plane, while maintaining the 0.50-m distances below the water surface and at the bottom center of the buoy. Figure 21 is an image of one of the conical buoys and its associated dimensions.

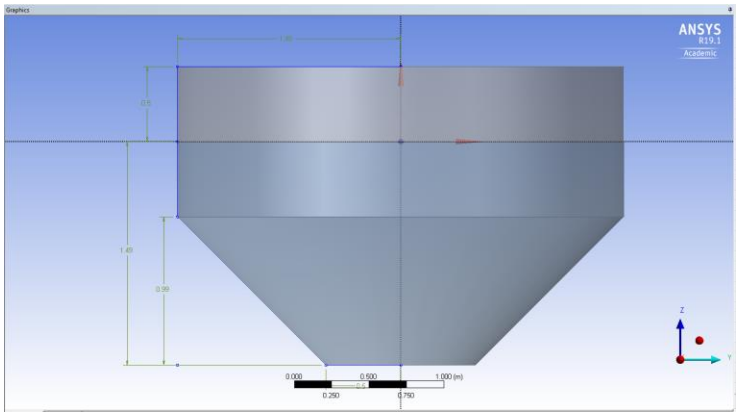

Figure 21. Conical buoy

The final design was that of an inverted arc along the chamfer line of the conical buoy. That is, the arc of same radius as the hemispherical buoy was drawn as a mirror image of the hemispherical arc with the chamfer line serving as the mirroring axis. This resulted in a shape similar to an inverted Sorry® game piece. The idea of this shape was to reduce the area of the wetted surface and provide an alternate curvature in an attempt to show a trend or relation between all the shapes with respect to surface area of the wetted surface and curvature. The pinched cone buoy is shown here in Figure 22.

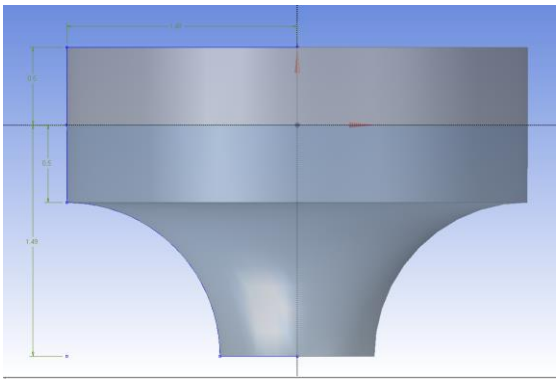

Figure 22. Pinched cone buoy

For each of the geometries, the distance above the water line is the same, as is the draft. The parameter being tested is simply the shape of the bottom of the buoy. When designing the buoys in ANSYS, it is critical to create the geometry correctly in order for the Aqwa analysis system to be able to evaluate the body. The creation of a 3D object from the 2D profile must be done using the thin surface option in Design Modeler, not the solid body option. Aqwa will not recognize a solid body and the analysis cannot proceed. Additionally, because of the way the solver analyzes the oscillating body, the body must be sliced along where the water line is intended. Once accomplished, the two bodies can then be formed into a new part, having two sub-components. A sample of the Design Modeler project tree is seen in Figure 23.

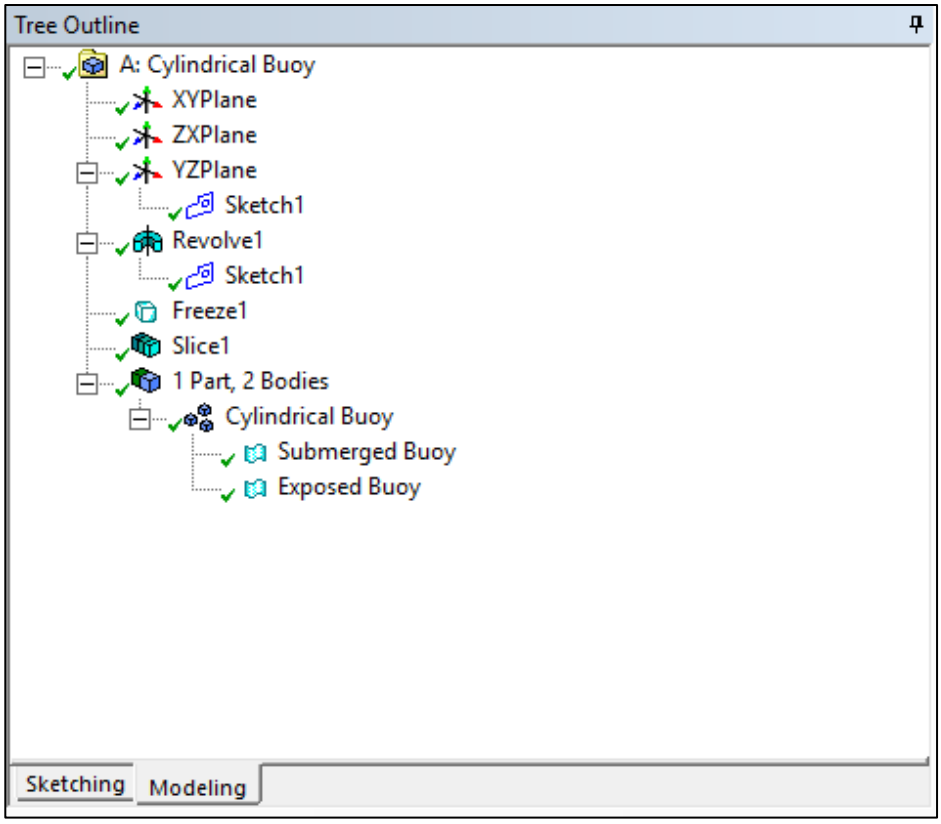

Figure 23. Details of geometry in ANSYS Design Modeler project tree

3.2 Hydrodynamic Diffraction

Once the buoy geometry was finalized in Design Modeler, it was imported into the Aqwa Hydrodynamic Diffraction analysis system where the analysis of the hydrodynamic parameters could be performed. In order to successfully perform the analysis in Aqwa, the initial and boundary conditions had to be established. For the follow-on time response analysis, the buoy also had to be moored to the ocean floor. This was accomplished using a linear cable with a prescribed axial stiffness. In the optimization of buoy performance, each of the individual components should be optimized, to include axial stiffness for different conditions. However, to keep focus on the geometry specifically, a stiffness of 500 N/m was selected. This provided enough stiffness so that the buoy did not drift more than a few meters from the original spot on the free surface plane and proved to be an effective value wherein a sinusoidal oscillation

of the buoy was achieved under various other sea states. Higher values for axial stiffness were attempted but the result was that the buoy ended up becoming submerged fully under water. Lower values were also attempted but the results were such that the buoy drifted a considerable distance and resulted in inconsistent values of motion. A depiction of the model set up with the buoy and mooring line are seen here in Figure 24.

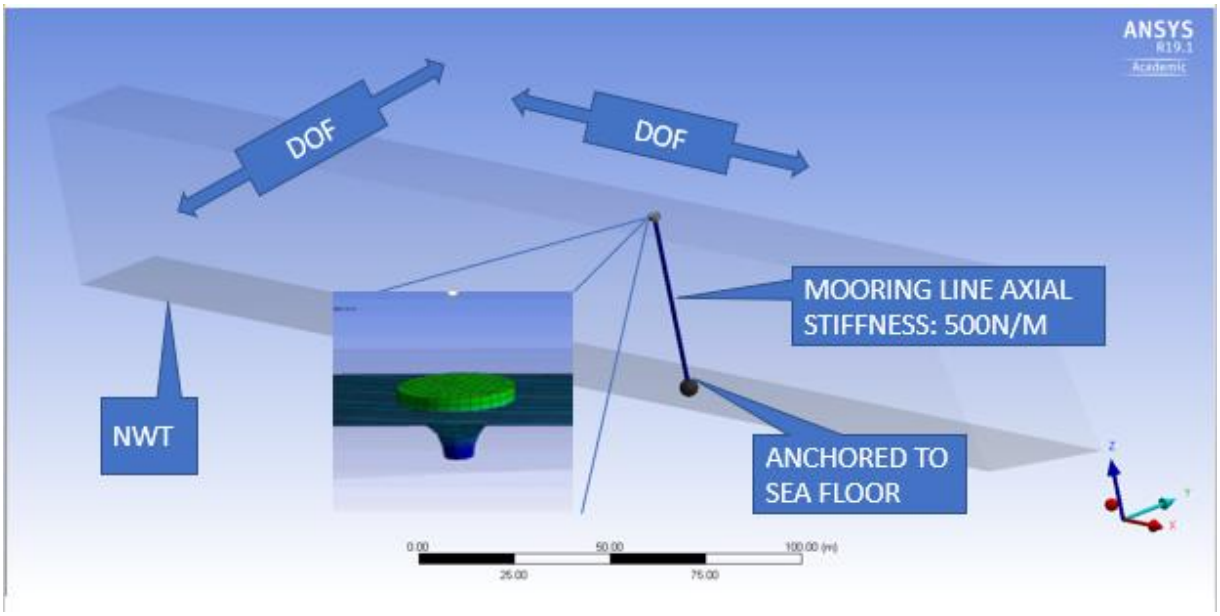

Figure 24. Numerical wave tank with buoy and mooring line

3.3 Mesh selection

The mesh selection for the model requires attention for the analysis to be effective. The program will give an error message unless the element size and defeaturing tolerance are correct in accordance with the frequencies selected for the analysis, and the frequencies must be selected appropriately in order to allow the program to analyze convolution in the system. For the Conical buoy with a diameter of 2.98m, the maximum element size is chosen to be 0.75m, which satisfies the requirements, seen in Figure 25.

Details

Details of Mesh	
Defaults	
Control Type	Basic Controls
Mesh Parameters	
Defeaturing Tolerance	0.25 m
Maximum Element Size	0.75 m
Maximum Allowed Frequency	0.756 Hz
Meshing Type	Program Controlled
Generated Mesh Information	
Total Nodes	310
Total Elements	308
Diffracting Nodes	215
Diffracting Elements	202
Line Body Nodes	0
Line Body Elements	0
Field Points	0

Figure 25. Details of mesh settings

3.4 Initial conditions

For the hydrodynamic diffraction of the various buoys, the initial conditions were selected in accordance with the previously discussed establishment of buoy diameter. In order to determine how different buoys reacted under various sea states, the wave frequency was established based on the hourly buoy data for the Gulf of Maine from NOAA [26] as selected from various buoys within the Eastern Maine buoy map, seen in Figure 26.

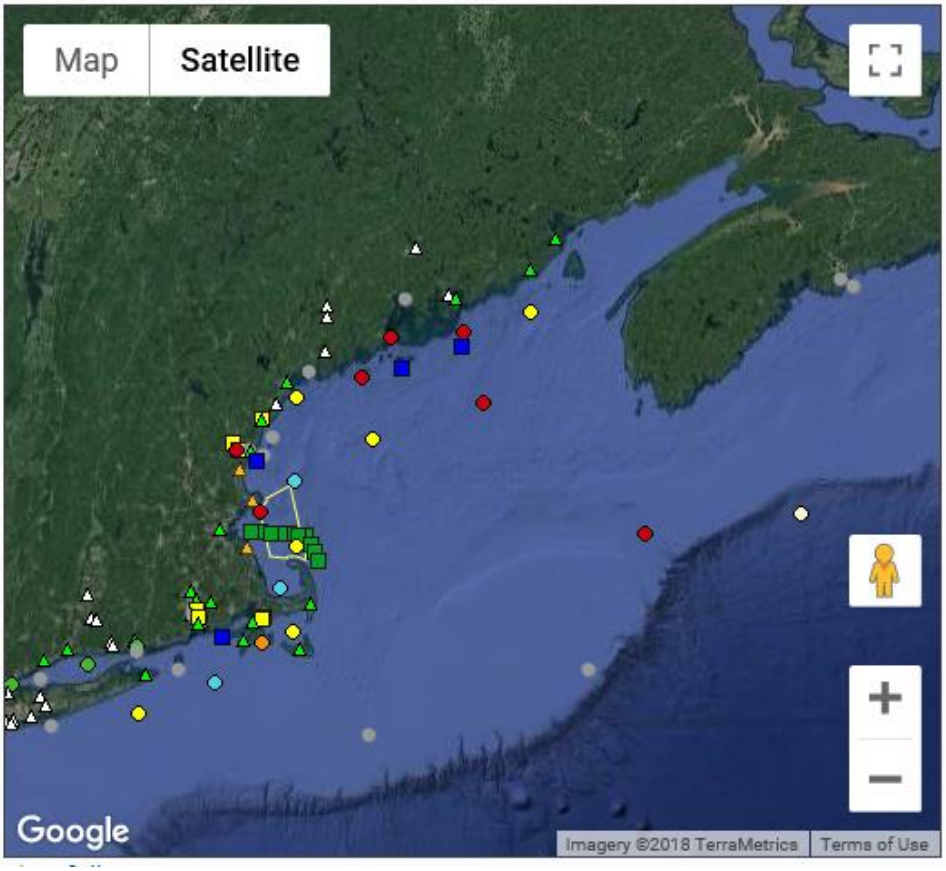

Figure 26. Buoys along the New England coastline [26]

Four different wave periods were chosen based of the variability of wave data on the coast at varying ocean depths. The shortest period observed was 4.6s and the longest period was 11s. An average wave period was plotted for a period of 6 months and the average of the entire period was 7.2s as seen here in Figure 27.

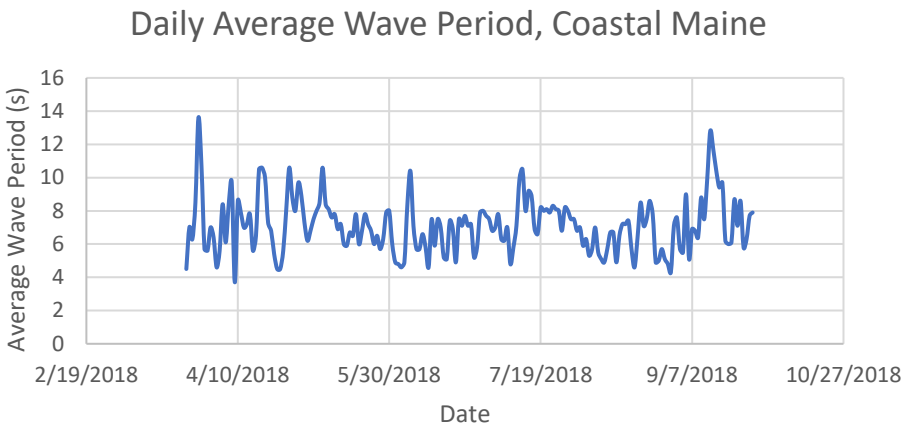

Figure 27. Coastal Maine wave period over six months

Additionally, although a height of 1m was chosen for the wave amplitude in order to ensure proper application of LWT, it can be seen here that the average wave height for the 6-month period was almost exactly the same, coming in at 1.03m. Figure 28 shows the average daily wave height for the 6-month period.

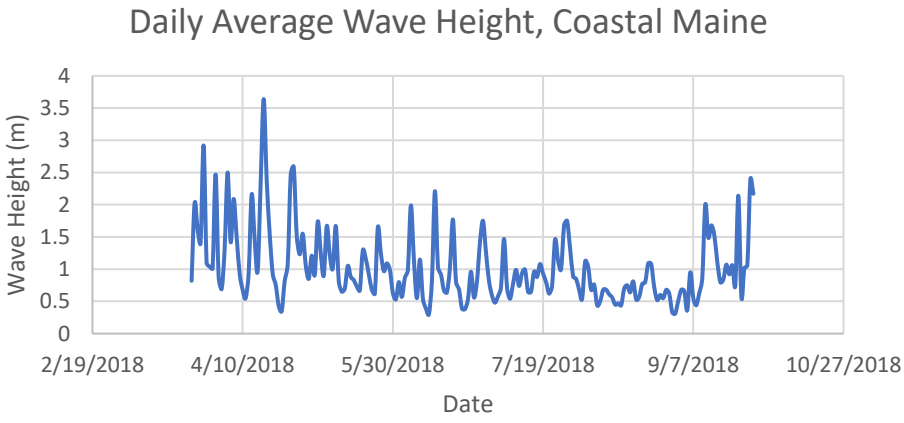

Figure 28. Significant wave height for coastal Maine buoy data

As clearly indicated by both graphs, there is a concern of intermittency when discussing the application of the wave energy converters. Seasonal variations in sea states are one of the major reasons the WEC industry has not taken off. Based on the given data, wave periods between 6 and 9s were used as a reasonable bandwidth. The model set-up and initial conditions of one trial of the hydrodynamic parameter analysis portions are shown here. An important note to point out for the analysis is that the "ignore modeling rule violations" option must be set to yes for the analysis, otherwise, Aqwa cannot complete it. Figure 29 displays some of the analysis settings for the program.

Details

Details of Analysis Settings	
Name	Analysis Settings
Parallel Processing	Program Controlled
Generate Wave Grid Pressures	Yes
Wave Grid Size Factor	2
Common Analysis Options	
Ignore Modelling Rule Violations	Yes
Calculate Extreme Low/High Frequencies	Yes
Include Multi-Directional Wave Interaction	Yes
Near Field Solution	Program Controlled
Linearized Morison Drag	No
QTF Options	
Calculate Full QTF Matrix	Yes
Output File Options	
Source Strengths	No
Potentials	No
Centroid Pressures	No
Element Properties	No
ASCII Hydrodynamic Database	No
Example of Hydrodynamic Database	No

Figure 29. Details of hydrodynamic response analysis settings

3.5 Hydrodynamic parameters and power output

The solutions to the hydrodynamic diffraction problem as previously discussed that are relevant to the solution of the equation of motion are the excitation force, approximated by the Froude-Krylov force, the added mass, and the radiation damping coefficient. The first part of the experiment was to run the hydrodynamic diffraction for the various buoy sizes across the different frequencies in order to determine the relevant parameters. It is worth noting that the hydrodynamic diffraction analysis results in the parameters for the buoy based on the dimensions of the buoy and are not affected by downstream analysis of the interaction of the buoy with different wave types or amplitudes. The excitation force solved for in the diffraction portion is used in conjunction with the wave amplitude selected with either a regular or irregular wave in order to solve the equation of motion. A discussion of the results of the hydrodynamic parameter analysis is presented in the next section.

The hydrodynamic diffraction was conducted for each of the four buoy shapes and for each shape, four different diameters were also tested. Once completed the hydrodynamic response could be conducted for each of the buoys for various sea states. Both regular and irregular wave response was conducted for each buoy. For the regular wave response, the default analysis settings were sufficient for the larger diameter buoys, but for the smaller diameter buoys with a smaller element size, it was required to adjust the time step to 0.1s. Because of this constraint, the same time step was applied to all of the buoys, regardless of size. The duration of the analysis was set to 1000s. This provided a sufficient amount of time for the analyses to show appropriate levels of convergence. Throughout the optimization process, the duration was adjusted to determine if the response varied over a greater length of time.

As previously discussed, the excitation force, added mass, and radiation damping coefficients were solved in the hydrodynamic diffraction portion of the analysis. In the hydrodynamic response analysis, the target of the experiment is to produce a simulated power capture. This is accomplished by first adding an additional radiation damping force with units of [kN/m/s] to the radiation resistance matrix in the z direction, seen in Figure 30.

Matrix Definition Data

	X	Y	Z	RX	RY	RZ
X	0.0 kN/(m/s)	0.0 kN/(m/s)	0.0 kN/(m/s)	0.0 kN/(°/s)	0.0 kN/(°/s)	0.0 kN/(°/s)
Y	0.0 kN/(m/s)	0.0 kN/(m/s)	0.0 kN/(m/s)	0.0 kN/(°/s)	0.0 kN/(°/s)	0.0 kN/(°/s)
Z	0.0 kN/(m/s)	0.0 kN/(m/s)	15 kN/(m/s)	0.0 kN/(°/s)	0.0 kN/(°/s)	0.0 kN/(°/s)
RX	0.0 kN.m/(m/s)	0.0 kN.m/(m/s)	0.0 kN.m/(m/s)	0.0 kN.m/(°/s)	0.0 kN.m/(°/s)	0.0 kN.m/(°/s)
RY	0.0 kN.m/(m/s)	0.0 kN.m/(m/s)	0.0 kN.m/(m/s)	0.0 kN.m/(°/s)	0.0 kN.m/(°/s)	0.0 kN.m/(°/s)
RZ	0.0 kN.m/(m/s)	0.0 kN.m/(m/s)	0.0 kN.m/(m/s)	0.0 kN.m/(°/s)	0.0 kN.m/(°/s)	0.0 kN.m/(°/s)

Figure 30. Radiation resistance matrix

If the analysis was required to determine additional capability through surge or pitch, or even for rotational motion, then additional terms could be added to the radiation resistance matrix. This represents the simulation of adding a Power-Take-Off device somewhere in the system. For a fixed reference device, the PTO could be a hydraulic cylinder anchored to the ocean floor with the heave motion providing the linear motion of a piston cylinder.

The addition of this PTO force adds a term to the equation of motion and results in a different velocity of the buoy in oscillation. As more damping is added to the system, providing a force in the positive *z*-direction, the velocity of the buoy slows. To counteract that, a supplemental mass is added to the mass matrix in the *z*-direction, simulating an additional spring force which speeds up the buoy in heave only, shown in Figure 31.

Matrix Definition Data

	X	Y	Z	RX	RY	RZ
X	0.0 kg	0.0 kg	0.0 kg	0.0 kg.m/°	0.0 kg.m/°	0.0 kg.m/°
Y	0.0 kg	0.0 kg	0.0 kg	0.0 kg.m/°	0.0 kg.m/°	0.0 kg.m/°
Z	0.0 kg	0.0 kg	1000 kg	0.0 kg.m/°	0.0 kg.m/°	0.0 kg.m/°
RX	0.0 kN.m	0.0 kN.m	0.0 kN.m	0.0 kN.m²/°	0.0 kN.m²/°	0.0 kN.m²/°
RY	0.0 kN.m	0.0 kN.m	0.0 kN.m	0.0 kN.m²/°	0.0 kN.m²/°	0.0 kN.m²/°
RZ	0.0 kN.m	0.0 kN.m	0.0 kN.m	0.0 kN.m²/°	0.0 kN.m²/°	0.0 kN.m²/°

Figure 31. Supplemental Mass Matrix

The purpose of these actions is to optimize the velocity of the buoy as it oscillates in heave and maximize the power by applying that velocity against the resistance of the PTO damping force, as previously discussed. Once the parameters are added, the buoy is tested in response to a regular wave with an amplitude of 1m and a period is chosen depending on the diameter of the buoy. The response of the power capture of the device is calculated by the hydrodynamic response analysis system in Aqwa. In the details of analysis settings there are three options for analysis type and there are four options for the settings, regular wave response, irregular wave response, irregular wave response with slow drift, or slow drift only.

Due to the objectives of this study, the primary method for comparison of the different buoys was to use a regular wave. The rationale for this is the assumption that an irregular wave, being simply a complex superposition of a number of regular waves with different amplitudes, frequencies, and angles of incidence will produce forces on an oscillating body proportional to each of the individual regular components and the response of the oscillating body in turn will be proportional to those sub-components as seen in Figure 32.

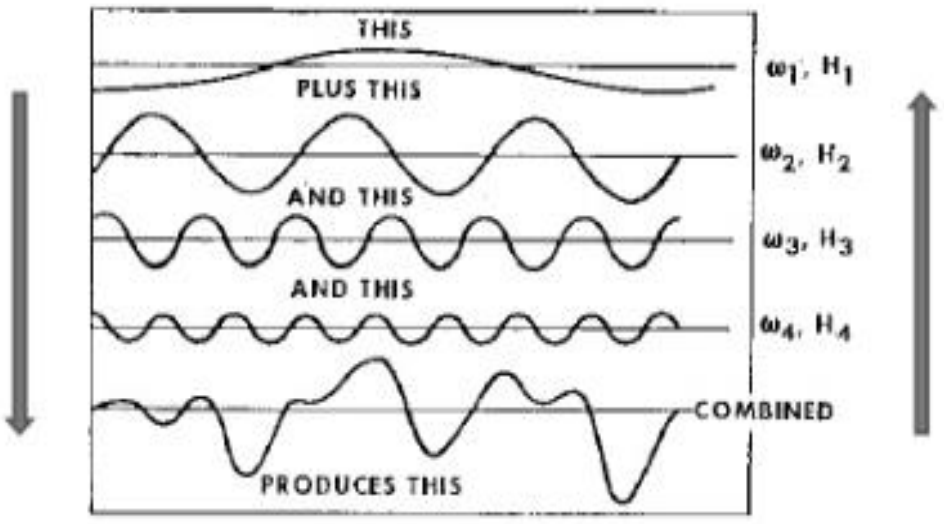

Figure 32. Superposition of regular waves to create irregular waves [33]

Therefore, an oscillating body that performs better in regular waves will, in theory, also perform better in irregular waves. The power performance of each of the buoys in irregular waves is examined in the last part of the experiment for reference but does not serve as the main focus for the experiment.

3.6 Optimization in regular waves

The selection of the optimal shape for the geometry of the buoy is predicated on the notion that all the modifications to optimize the performance of the buoy, that reasonably can and should be accomplished prior to deployment of the buoy, are completed based on the results of the experimental studies. That is to say, if the deployment of a wave energy device is proposed for an area with a known sea state, the PTO capture device damping coefficient as well as the supplemental mass can be set prior to launching the device. A comparison of the geometry alone, without accounting for the optimization of the PTO damping and supplemental mass, provides no substantial information from which to make a decision. The selection of a fixed PTO damping and supplemental mass optimized to each shape is, however, only relevant in the

comparison of the geometries. It has been shown by numerous researchers that in wave energy device development a reactive or predictive damping based on the sea states can improve performance significantly. The development of those systems can and should be further established once a geometry is selected.

The optimization of the power performance of the wave energy devices studied in this experiment was attempted in three distinct ways, one of which resulted in the method that was used successfully across the remainder of the experiment. The first method was used based on the previously discussed selection of the draft of a device based on the optimized heave frequency being matched to the frequency of the incident wave. The hydrodynamic parameters were found for each device, then based on those numbers, a supplemental mass was calculated using Equation 9.

For example, the structural mass for the cylindrical buoy with a diameter of 2.98m was calculated as 10,171 kg. The added mass calculated by Aqwa came out to 7,249 kg. Then plugging into Equation 9, a supplemental mass of 44,785.22 kg was determined. One reason this value is so high is that the optimal draft for the device without supplemental mass would have been approximately 9 m. For a sea state with a wave period of 11 s, the optimum draft according to the same equation is over 30 m. Although not impossible to construct and test a buoy of that draft, the amount of surface area that would be affected by the changing of the shape of the bottom surface would become orders of magnitude less than the cylindrical surface that was in contact with the water. Additionally, the velocity potential is highest at the surface of the water, so an extended buoy likely does not take advantage of that property.

In the example above, the supplemental mass of 44,785.22 kg was included in the properties of the buoy. The validation of the calculation is presented by the Aqwa solver if the “Pressures and Motions” option is selected in the solution branch of the hydrodynamic diffraction. Using the specific supplemental mass, not one percent higher or lower, the pressures and motions produces a phenomenon in the results that shows the buoy achieving, in the example of the hemispherical buoy in Figure 33, an amplitude of 28m

above the surface. This information is seemingly valuable at first, but upon further exploration, only applies to solving for the optimum added mass for an oscillating body in heave with no external PTO applied.

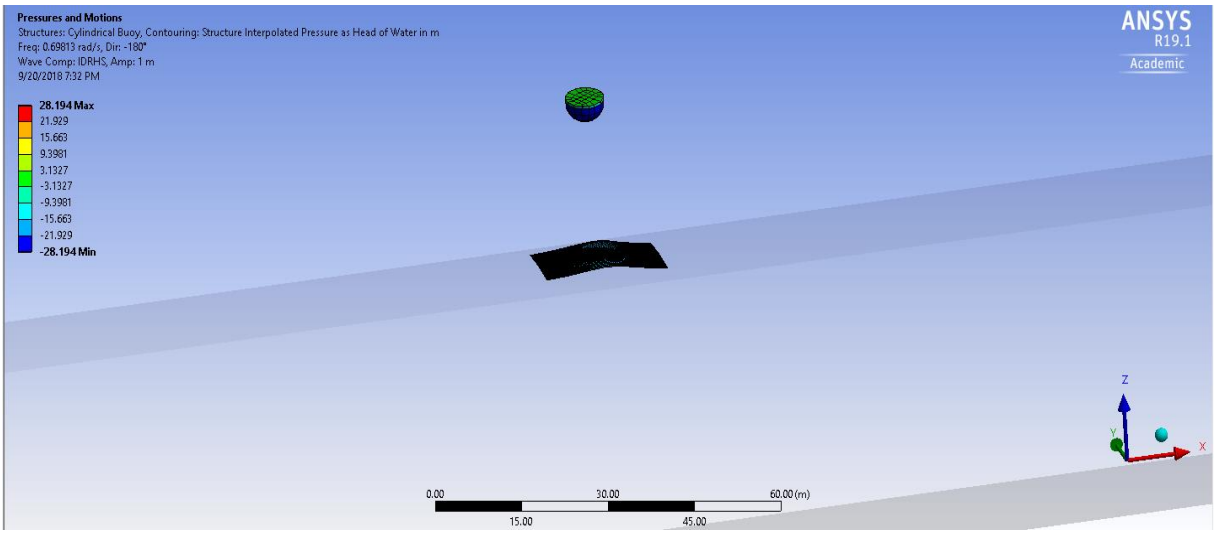

Figure 33. Oscillation of heaving buoy in resonance

When the addition of a PTO damping coefficient was applied using this method, the power capture was only 61% of that found with the final method. The power curve for this method is seen in Figure 34.

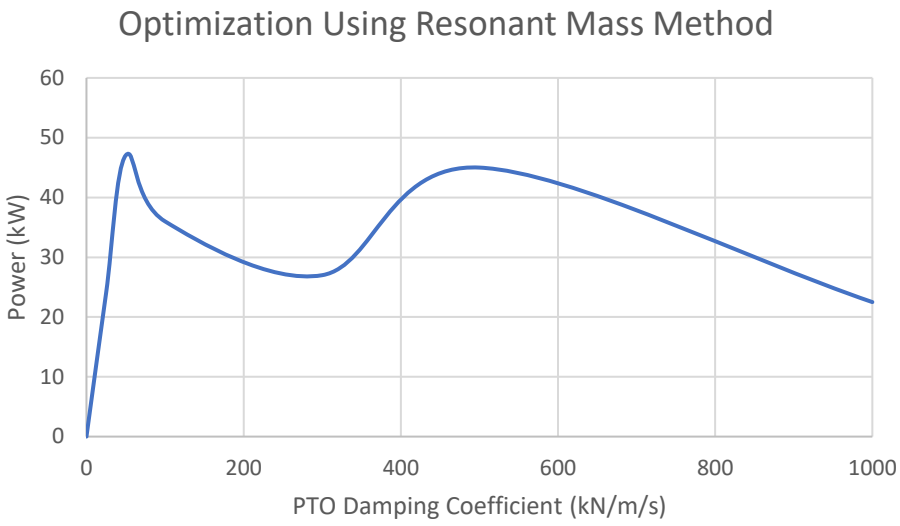

Figure 34. Power optimization using resonance mass

The second method, based on the understanding of the terms involved in the equation of motion and the hydrodynamic parameters that are available to be added in Aqwa, uses an iterative process with the PTO damping coefficient as the first parameter and the supplemental mass as the second. The definitive purpose behind the WEC is the extraction of energy through the PTO device, so it follows logically that as the external PTO damping is increased, the power captured also increases. The absorbed power is a product of the PTO damping coefficient and the velocity squared of the buoy, but as the damping increases the velocity decreases and so a power profile is created as a function of the PTO damping coefficient. This profile has a peak power associated with it but because the velocity term is squared when it dips below a certain threshold the resultant power begins to drop off. The power profile achieved for a hemispherical buoy of 6.70m is shown in Figure 34. The power peak occurs at a PTO damping coefficient of approximately 200 kN/m/s. It is important to recall that the velocity achieved at this point is neither the maximum nor the minimum for the range of damping coefficients tested. However, according to the formula, it does produce the highest amount of power, as shown in Figure 33.

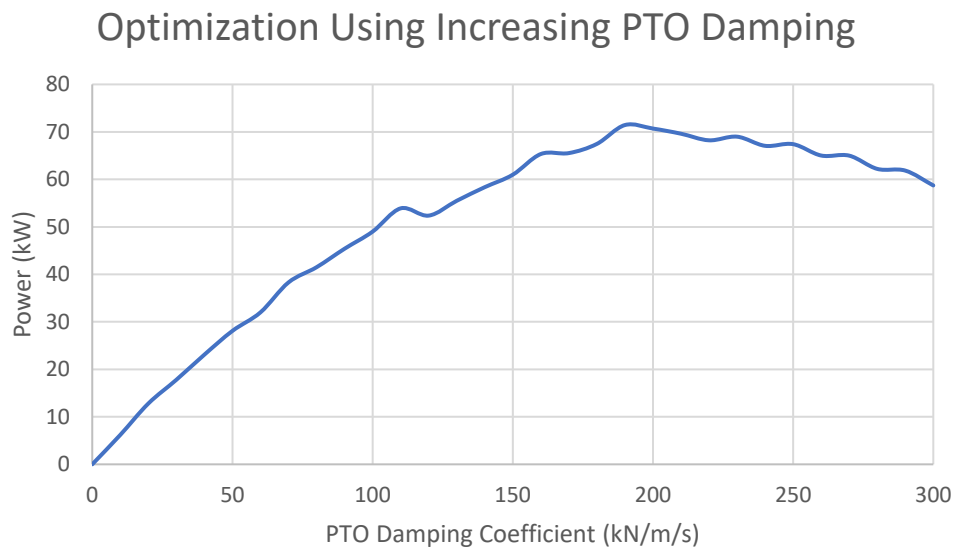

Figure 35. Optimization with increased PTO damping and no supplemental mass

The next step in this method was to take the value of the PTO damping coefficient that achieved the highest power output and test it against various supplemental mass values to see if the power output could be increased further. Several tests were run in this manner and the results were promising but the peak power achieved was about 5% lower than the peak power achieved using the third and final method. The power profile for this method is shown in Figure 36.

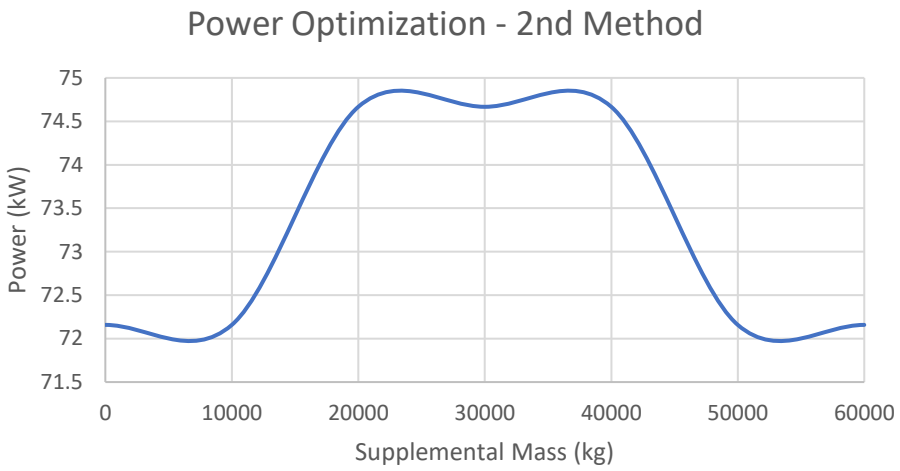

Figure 36. Power optimization with PTO damping as the primary parameter

Additionally, the PTO damping coefficient found in the final optimization method was just over half the amount found with this method. This factor could contribute to a reduction in overall cost if a lower damping coefficient is required in the system.

The third method of optimization which proved to be successful was a reversal of the second method and was based off the fact that changes in the velocity of the oscillating body has a more significant effect on the power than the PTO damping coefficient. For this method, a supplemental mass was added to the buoy in increasing increments and the velocity was recorded. After many iterations, the velocity profile of the buoy was determined and then the value of the supplemental mass that produced the highest velocity was then tested with increasing levels of external PTO damping. This method showed an overall improvement in the power capture of the device versus the two previous methods. The optimization flowchart for the chosen method in this experiment is shown in Figure 37.

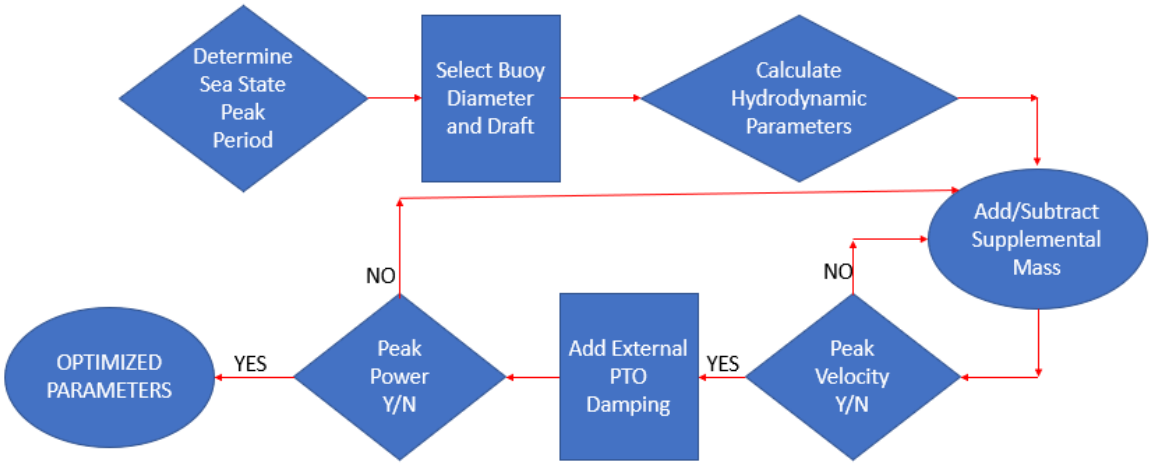

Figure 37. Optimization of PTO damping and supplemental mass for peak power

When the PTO damping coefficient was found that produced the highest power, the supplemental mass was checked for accuracy by adjusting it up to 10% of the initial value in either direction. The resulting power was found to be within a few percentage points of the first optimized value so served to validate the optimization method.

3.7 Response in irregular waves

Once the optimized power capture for each device was determined using the time response analysis for a regular wave, the final part of the experiment was to test how each of the optimized buoys would react to an irregular wave. In the second Hydrodynamic Response analysis system, the analysis system is set to irregular wave response, and a JONSWAP (H_s) irregular wave is inserted into the project outline. The spectral density function is created by the Aqwa solver according to the user-defined parameter set of peak period, significant wave height, and peak enhancement factor coefficient, γ. The duration of the trial was set to 1000s to provide sufficient time for the buoy to respond to the wave function. The resulting velocity

profile of the oscillating buoy was then examined, and the resulting peak and time-averaged power were calculated. To find the time-averaged power, the instantaneous velocity was recorded at each time step, in this case every 0.1 s, then input into Equation 21 to solve for the instantaneous power. The average power was then calculated for the duration of the experiment. An example of the spectral density function is shown in Figure 38.

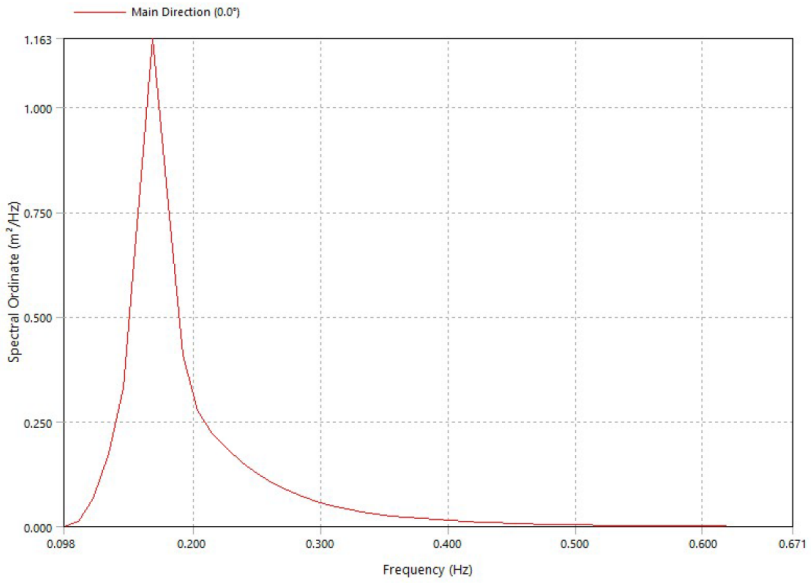

Figure 38. JONSWAP spectral density function determined in Aqwa

Through the various methods of the experiment, the following was examined: 1) the hydrodynamic parameters for each buoy shape and diameter, 2) the peak power and time-averaged power in regular waves, and 3) the time-averaged power for response in an irregular wave. Based on the data collected some significant conclusions about the different models can be drawn.

CHAPTER 4

RESULTS AND DISCUSSION

4.1 Excitation forces based on size

The goal of this experiment was to attempt to discern whether a partially submerged buoy oscillating in heave would benefit from the optimization of the geometry of the bottom surface in such a way as to show at least a 10% higher performance in power capture compared to buoys of other shapes. The method of determining the optimized power capture of the different devices required first that the hydrodynamic parameters be solved using the equation of motion and the radiation–diffraction method utilized in linear wave theory. The three parameters concerned in this experiment are the excitation force, the radiation damping coefficient, and the added mass.

The excitation force is approximated by the Froude-Krylov force and is the first parameter that was examined. As previously described, the excitation force is the integration of the velocity potential multiplied by the normal force acting on the body. In this case, the excitation force acting in the heave direction only was the main concern as that is the force that was applied against the PTO. The simulation covered the entire range of wave periods that could be expected in the coastal Maine region. The first shape examined was the cylindrical buoy. The graph clearly shows the excitation force increased as the wave period increased for each device and that the force was significantly higher for each succeeding diameter of buoy. At the very shortest of the wave periods there was essentially no difference in force, but wave periods of 2 to 3s are not found in any of the wave data researched and merely serve as an initial condition for reference. As the period increased, the differences became more pronounced. The excitation force acting on the largest buoy of 6.70-m diameter was 5 times higher than for that of the 2.98-m diameter buoy. So, the forces acting on the buoy increased almost 250% faster than the diameter. Because it is known that the excitation force is proportional to the surface area of the wetted surface of the buoy, it follows that the

increases in force would be exponential as diameter increases. Additionally, as shown in Figure 39, the excitation force began to level off at around T=13s, a very long period for real-world conditions.

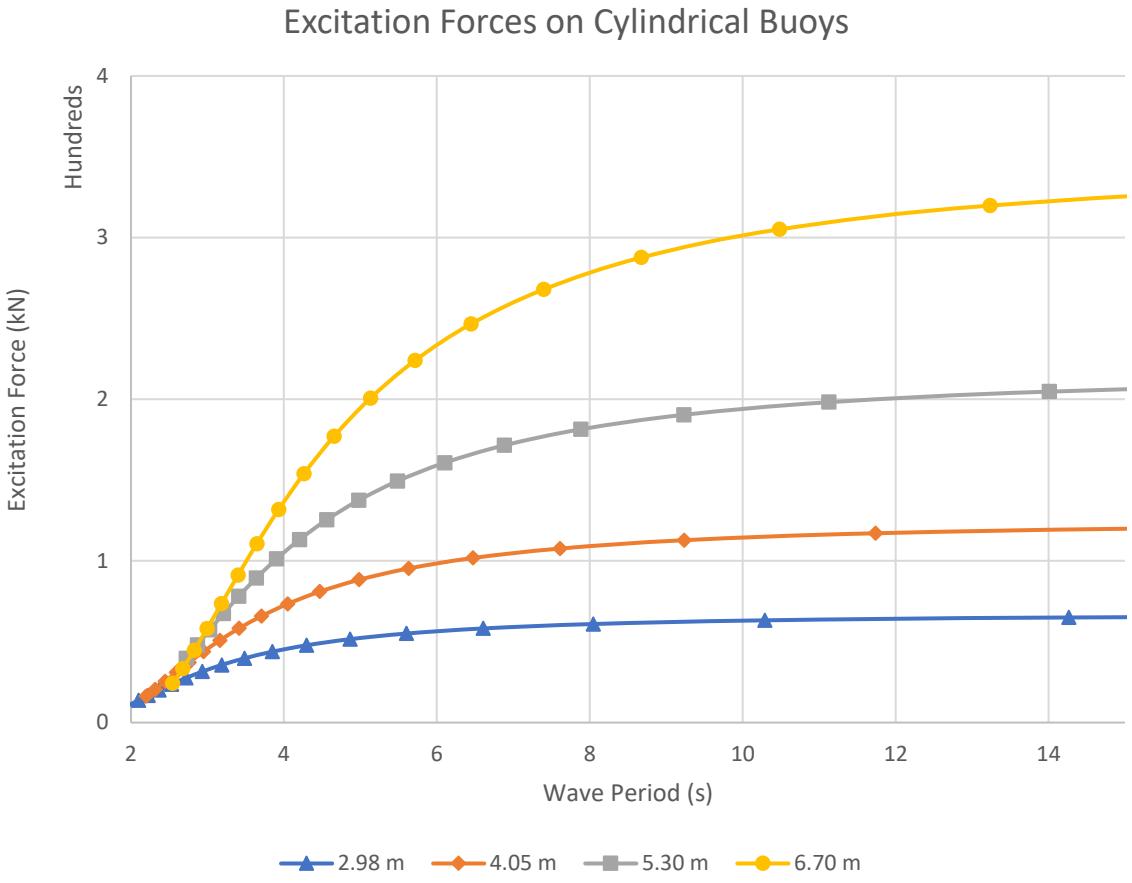

Figure 39. Excitation forces on cylindrical buoys of increasing diameter

The hemispherical buoy is the next shape tested, and the results are seen here in Figure 40.

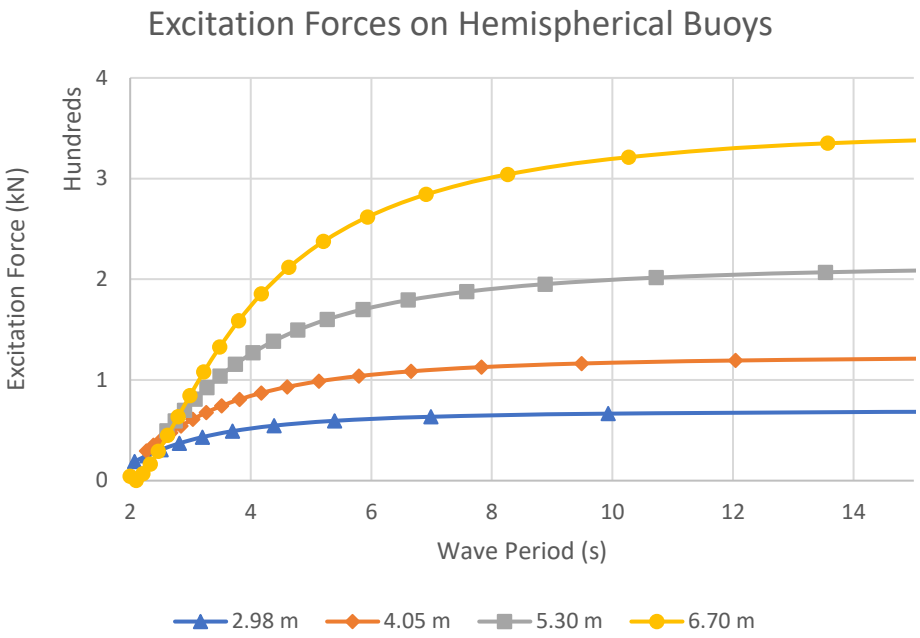

Figure 40. Excitation forces on hemispherical buoys of increasing diameter

The same trend of increasing forces, with both the conical and pinched cone shapes, is also shown in Figures 41 and 42.

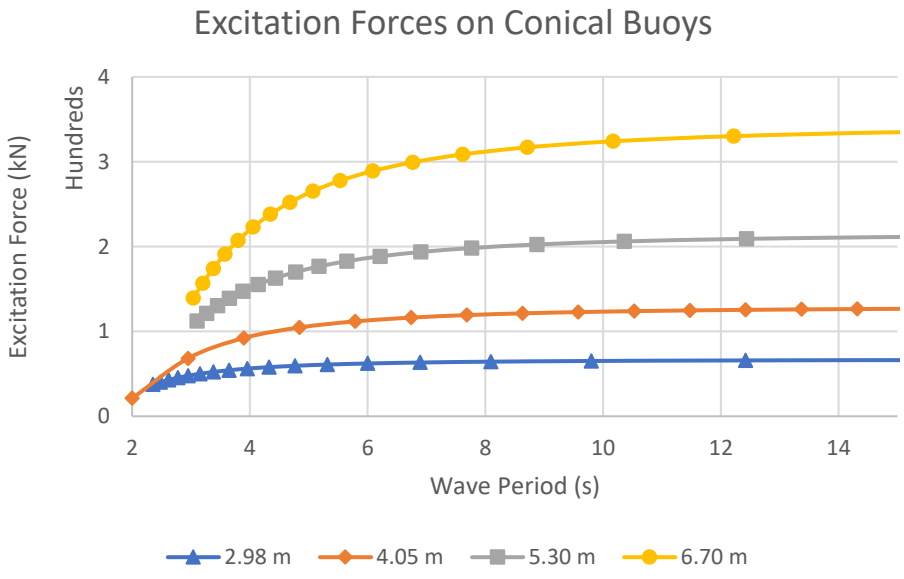

Figure 41. Excitation forces on conical buoys of increasing diameter

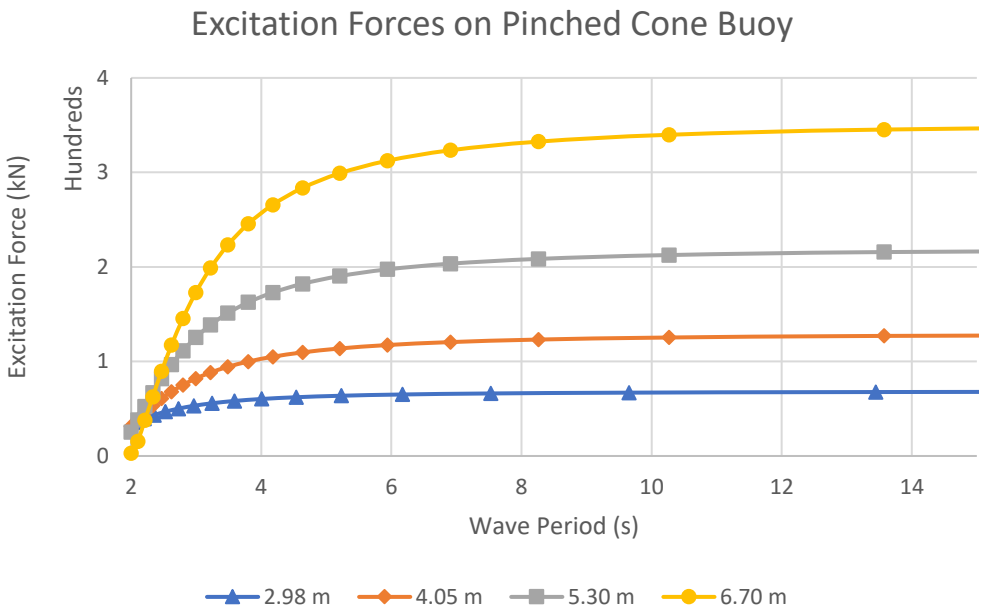

Figure 42. Excitation forces on pinched cone buoys of increasing diameter

The conclusions that can be drawn from this first set of data without consideration of other factors is that if excitation force is the determining factor in performance, the first option is going to be to construct a WEC with as large a diameter as possible. But this conclusion can only be relevant if there is a relationship between excitation force and overall performance. The next set of graphs uses the same data points, but in consideration of the excitation forces acting on the body relative to shape instead of diameter.

4.2 Excitation forces based on geometry

Figure 43 shows that there is a difference in the excitation force on buoys of the same diameter but with different geometries. The pinched cone shape shows a slight advantage, followed by conical, hemispherical, and cylindrical. The difference is more pronounced at smaller wave periods but converges to a 3% difference between the highest and lowest values at the longest wave period.

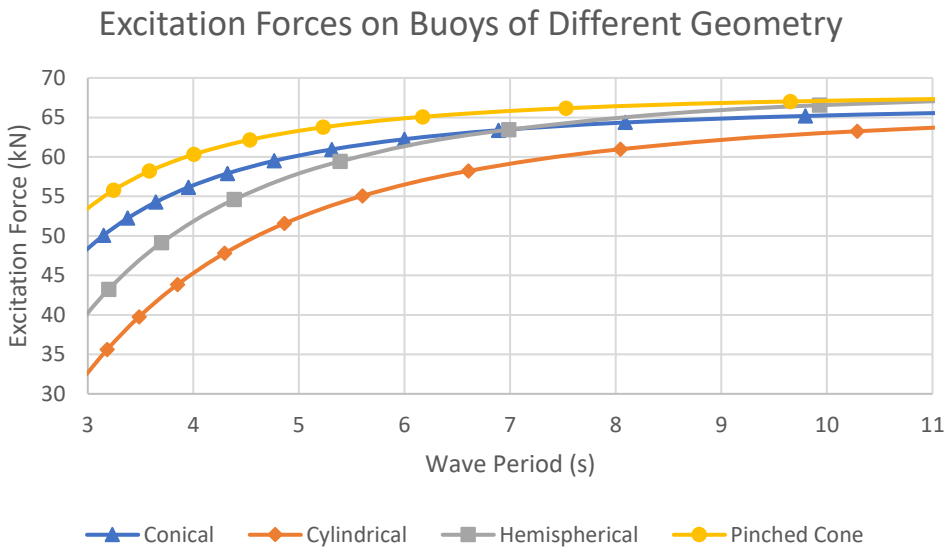

Figure 43. Excitation forces on different buoy shapes with a diameter of 2.98m

Figures 44, 45, and 46 show the remaining buoy sizes and the excitation forces acting on the buoys of different geometries.

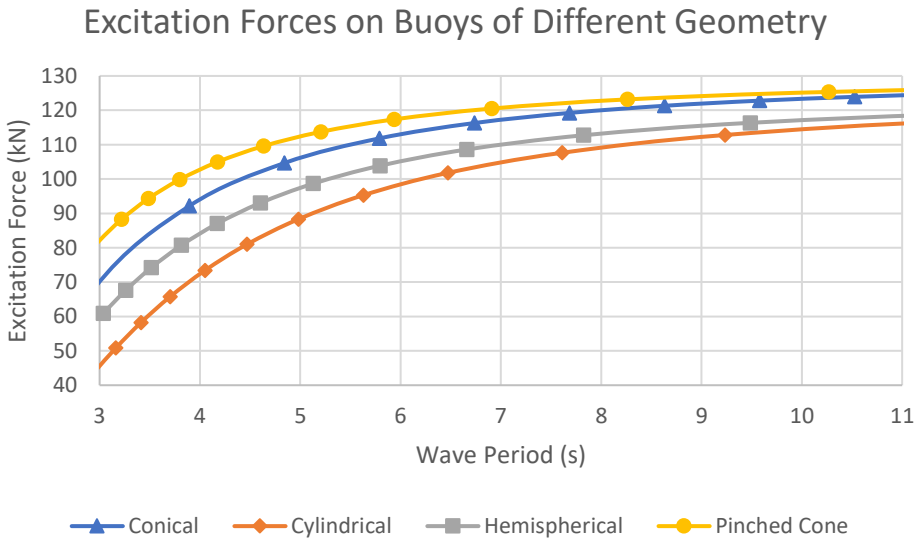

Figure 44. Excitation forces on different buoy shapes with a diameter of 4.05m

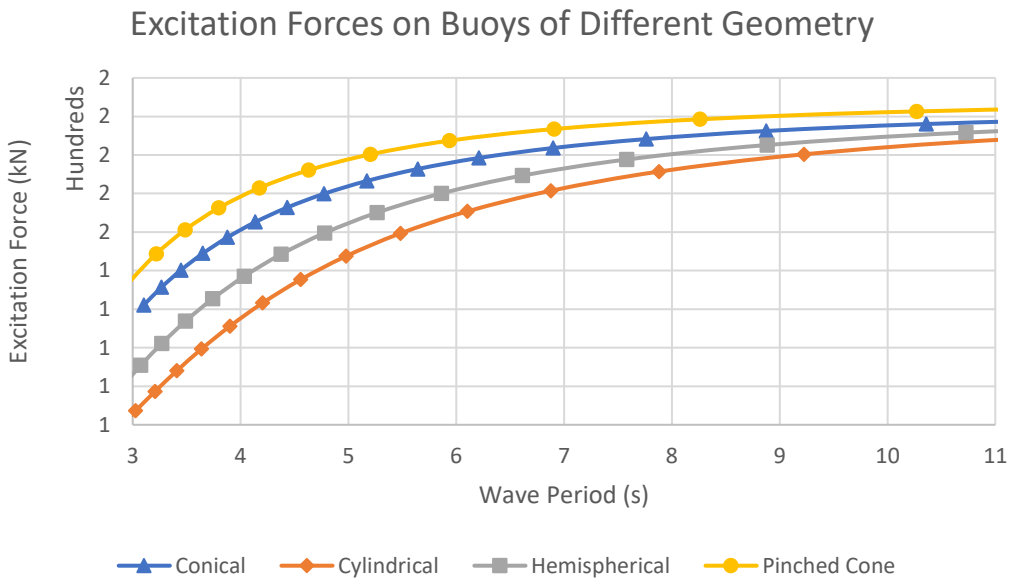

Figure 45. Excitation forces on different buoy shapes with a diameter of 5.30m

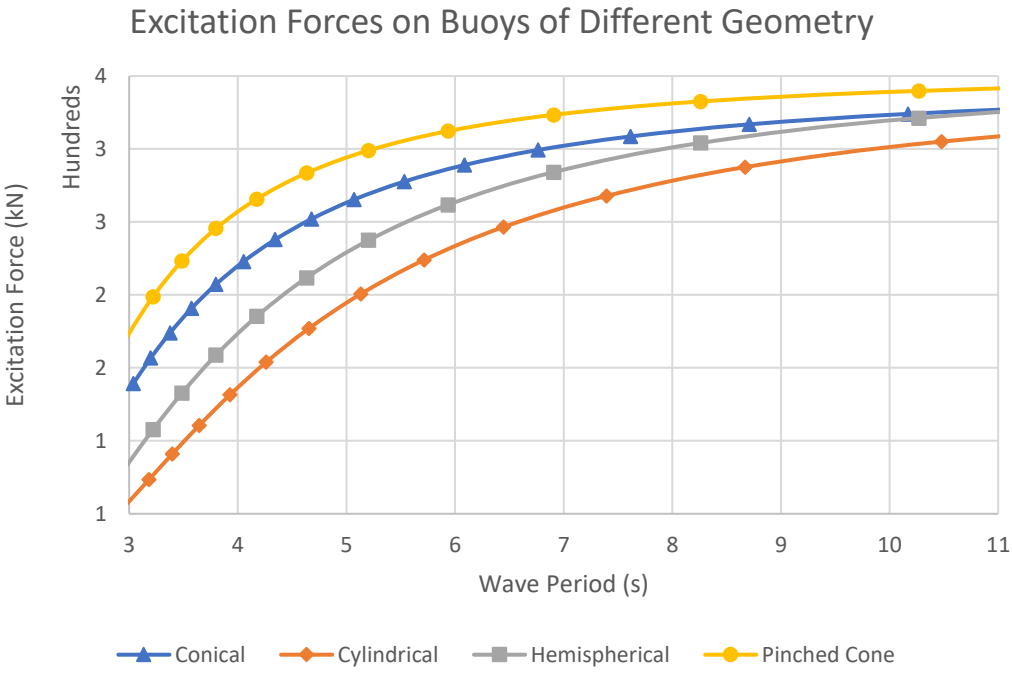

Figure 46. Excitation forces on different buoy shapes with a diameter of 6.70m

The trend remains identical in each of the figures, each showing the excitation forces acting on the buoy increasing as the geometry changes from cylindrical to hemispherical, conical, and finally, to the pinched cone. This does not concur with the theory that the excitation force increases proportionally with the surface area of the wetted surface as previously discussed. The surface area of the different buoy shapes is shown in the Table 2 for a buoy with a diameter of 4.05m.

Table 2. Wetted Surface Area of All Buoy Shapes

Buoy Shape	Surface Area (m^2)
Cylindrical	38.839
Hemispherical	27.896
Conical	24.361
Pinched Cone	23.109

It becomes clear that the excitation force depends on more factors such as the velocity potential as well as the angle of incidence with the wetted area and so cannot be attributed at present to one factor over the other.

4.3 Radiation damping coefficient

The next hydrodynamic parameter that was solved and analyzed was the radiation damping coefficient. This characteristic is frequency dependent and also affects the oscillation of the floating body. Any trends that can be deduced from the changes in the coefficient based on geometry may be helpful in further developing the best model. In Figure 47 the radiation damping coefficient for the smallest diameter buoy and all four shapes can be seen.

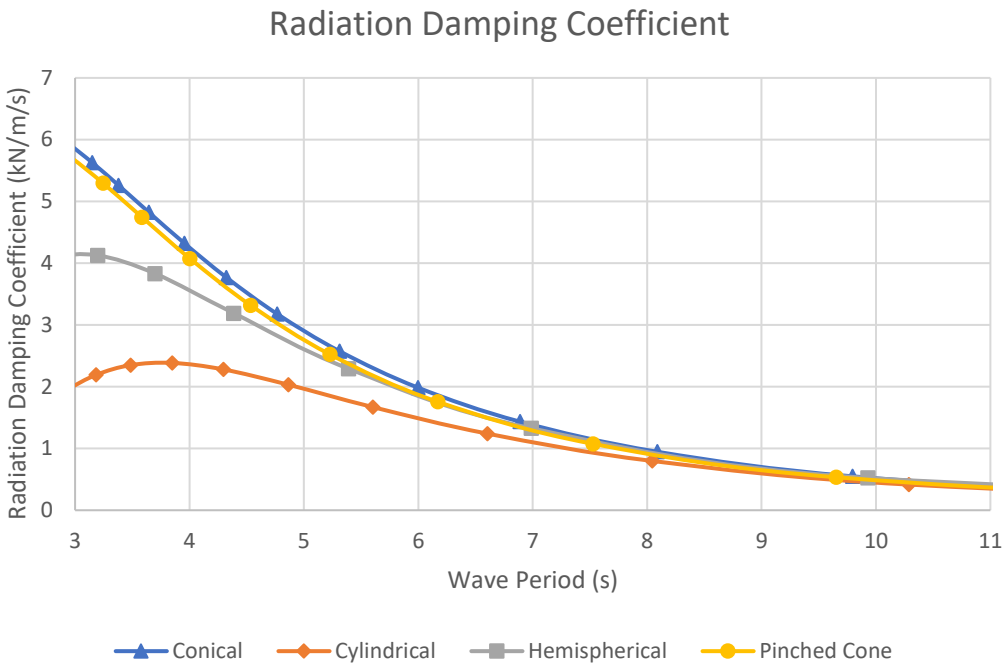

Figure 47. Radiation damping coefficient of different buoy shapes with a diameter of 2.98m

The radiation damping coefficient for the remaining three diameters are shown in Figures 48-50.

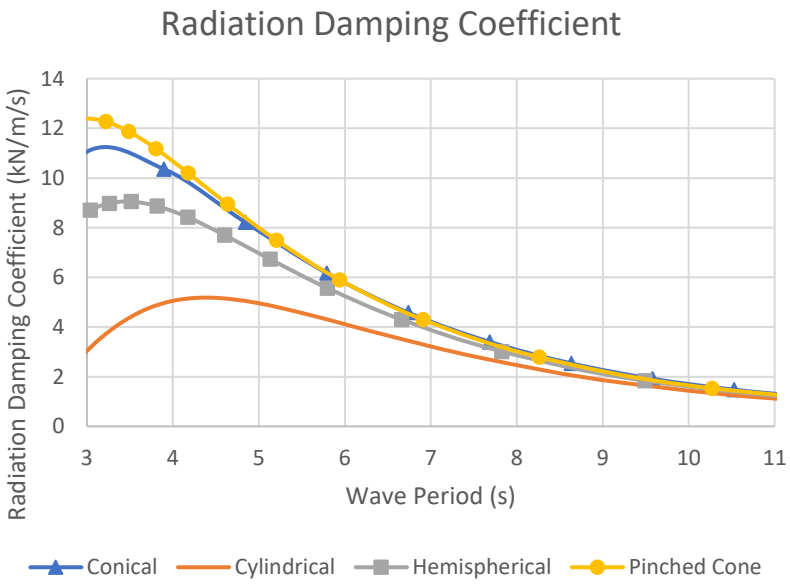

Figure 48. Radiation damping coefficient of different buoy shapes with a diameter of 4.05m

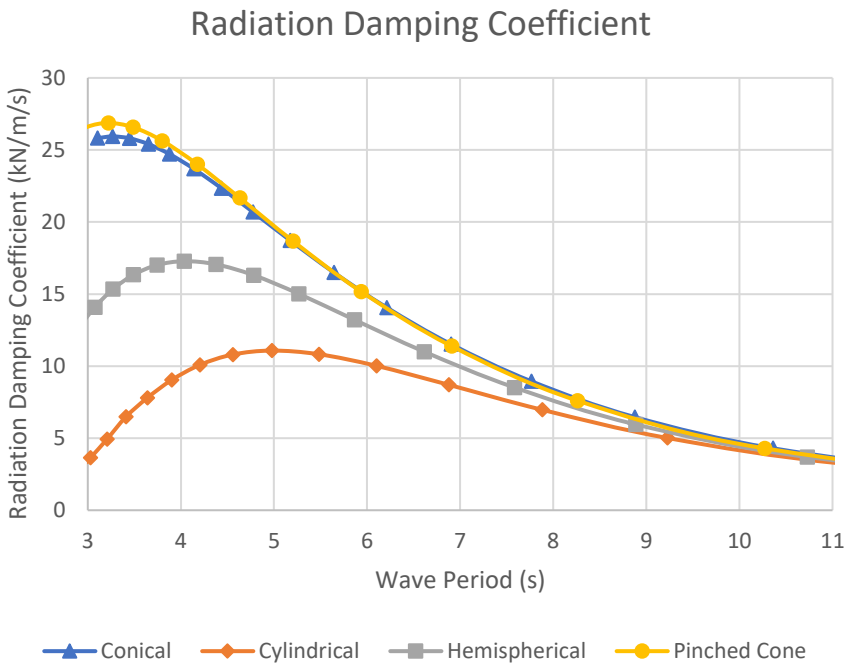

Figure 49. Radiation damping coefficient of different buoy shapes with a diameter of 5.30m

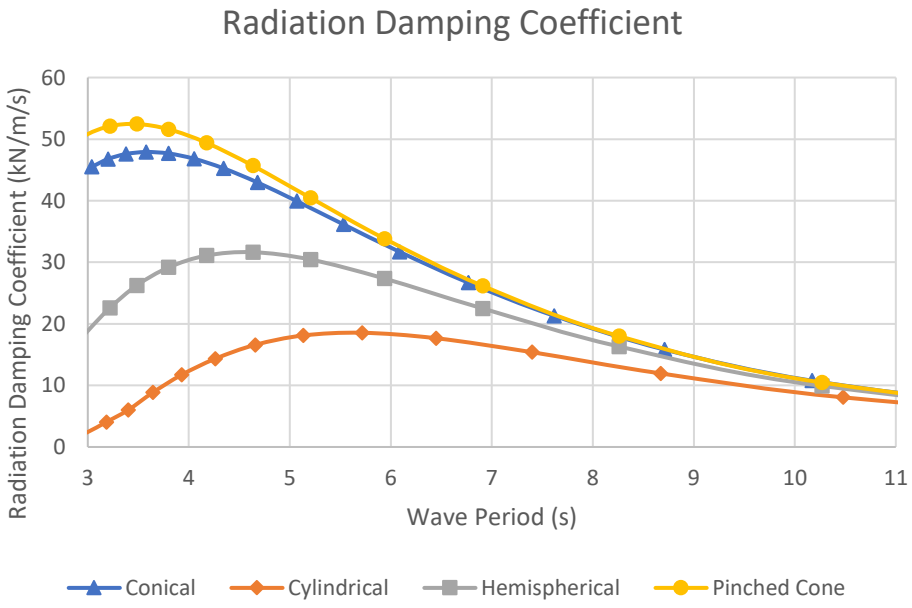

Figure 50. Radiation damping coefficient of different buoy shapes with a diameter of 6.70m

It was determined upon closer examination that the radiation damping values of the different shapes mirrors the excitation forces insomuch as the pinched cone shape predominantly stands out as the highest value, and the cylindrical the lowest. The only outlier in this trend is the radiation damping occurring at a diameter of 2.98m, where the conical buoy is a fraction higher than the pinched cone across the entire range of wave periods. It is impossible at this juncture to provide an explanation of this result without further investigating, but as will be shown later, this parameter has a minimal impact on overall performance. Additionally, it can be seen in each of the graphs that the radiation damping converges very quickly when approaching a wave period of 7s to 9s such that the values for all the shapes are within 10% of each other. The only significant differences are seen in very short periods which, although possible, are much less likely in actual sea states.

4.4 Added mass

The last hydrodynamic parameter that was examined was the added mass. The Aqwa solver calculates and adds this mass to affect the harmonic response of the oscillating body so as to oscillate in phase with the incident wave to the greatest extent possible. The relevance of added mass may be limited to future discussions on overall cost and ease of manufacture of WECs but is worth referencing here because Aqwa requires this information to solve the hydrodynamic response. Figures 51-54 show the added mass for each of the buoys in the same manner as the other parameters. The added mass is highest in the cylindrical buoys in three of the four diameters, followed by the pinched cone, conical, and hemispherical buoys. This order is dissimilar to any of the others so does not immediately point to any conclusions about the overall performance of the buoys.

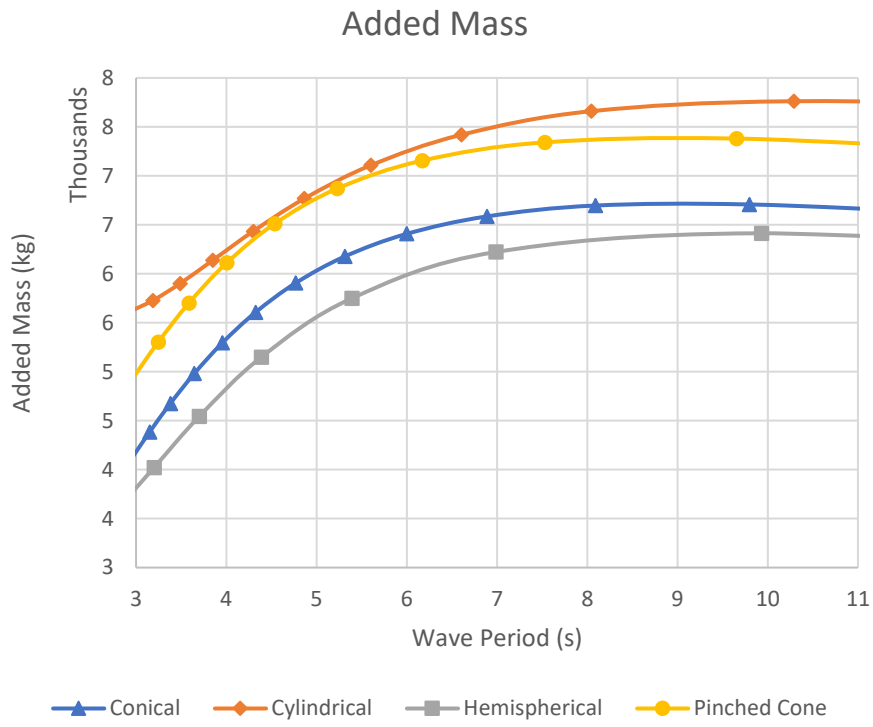

Figure 51. Added mass for different buoy shapes with a diameter of 2.98m

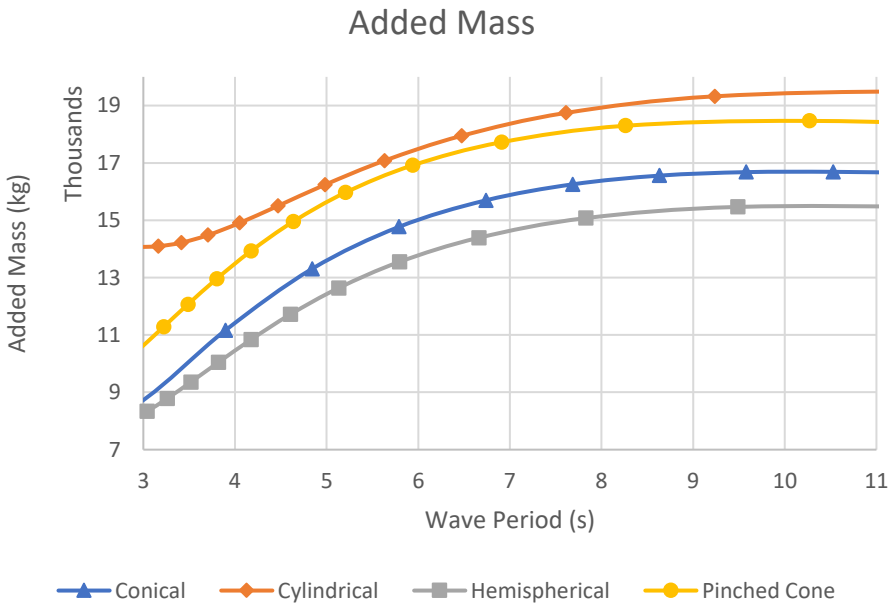

Figure 52. Added mass for different buoy shapes with a diameter of 4.05m

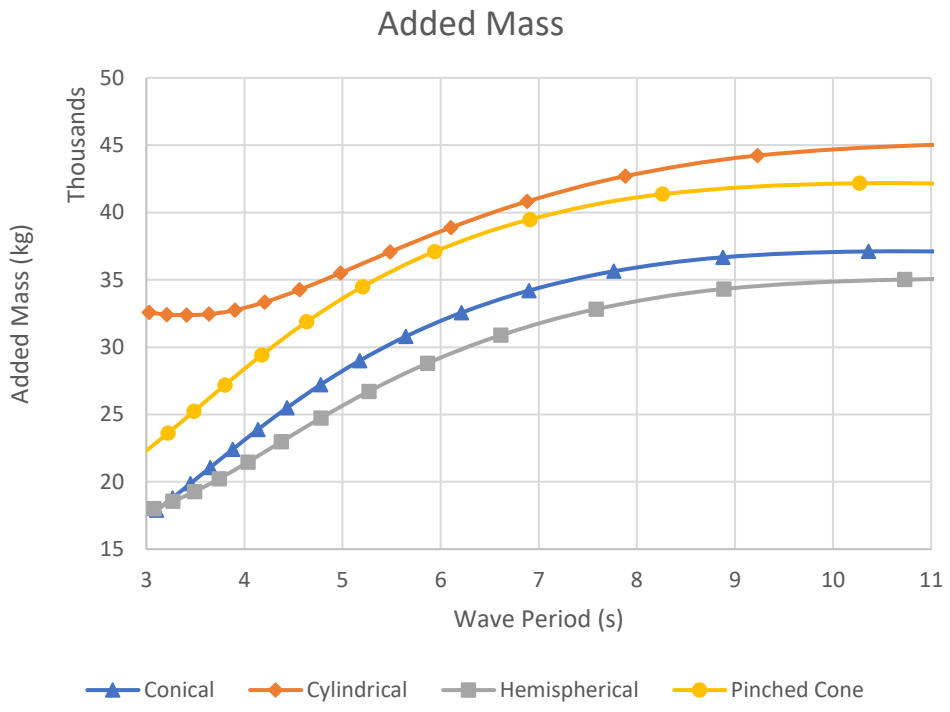

Figure 53. Added mass for different buoy shapes with a diameter of 5.30m

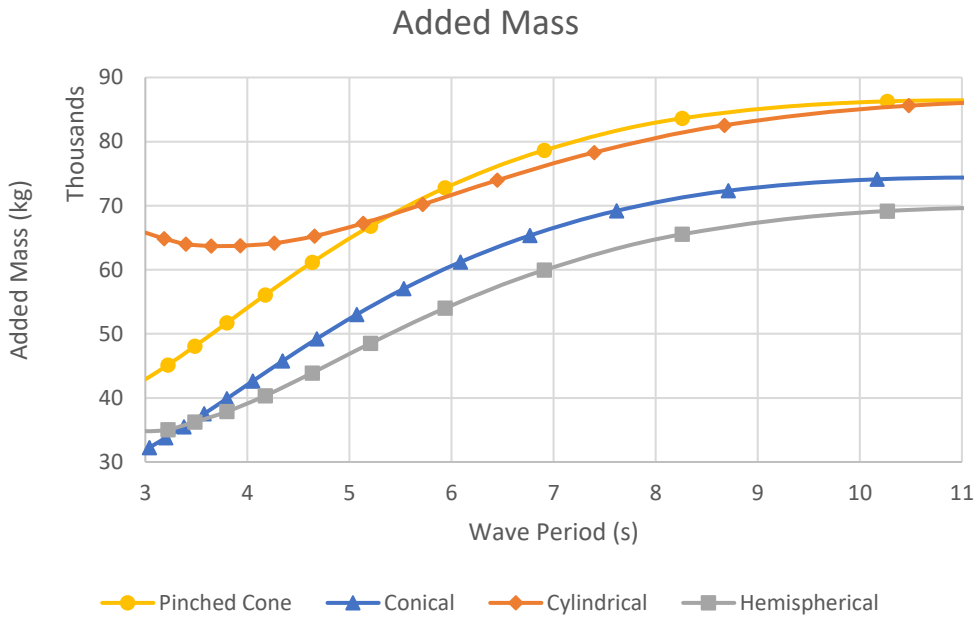

Figure 54. Added mass for different buoy shapes with a diameter of 6.70m

4.5. Optimization of velocity and peak power in regular waves

The next portion of the experiment was to conduct the hydrodynamic response of the oscillating buoy in a regular wave of 1m amplitude, with the frequency of the wave matched to the diameter of the buoy. That is, the buoy diameter was chosen based on the previously discussed principles of wavelength relating to maximum effective capture width ratio. Then using the dispersion relation in LWT, the frequency is calculated based on the wavelength.

This was the optimization portion of the experiment that determined the optimized power for each device at the specific wave frequency. The first step in the process, as discussed previously, was to optimize the added mass for the buoy. Starting at zero supplemental mass, the peak velocity was recorded, then supplemental mass was added in an incremental process to find the highest velocity. The results for the all the buoy shapes with a diameter of 2.98m are seen in Figure 55.

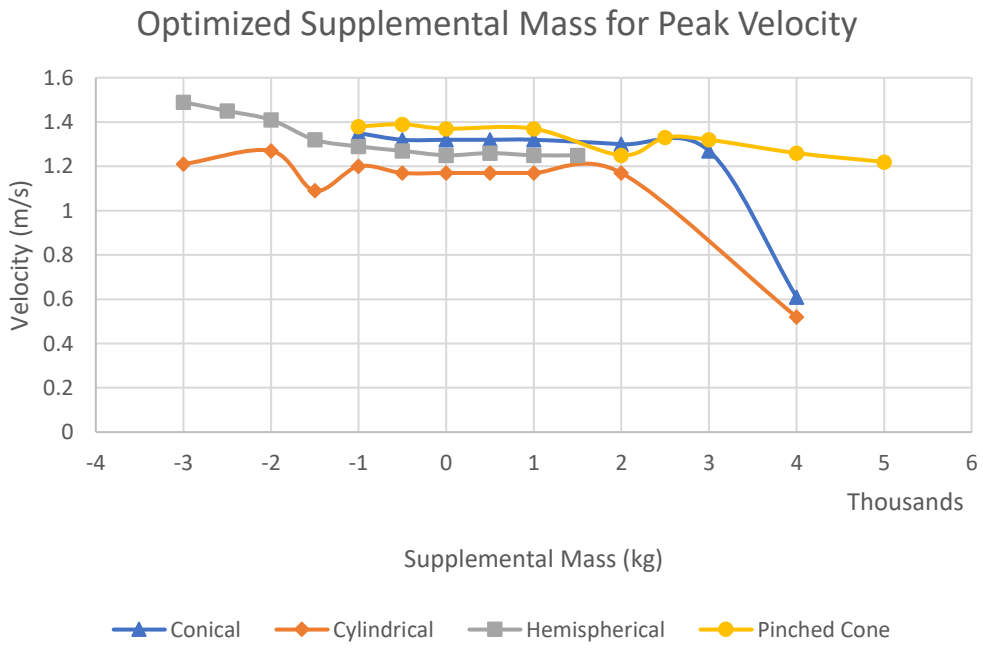

Figure 55. Optimized supplemental mass for peak velocity

The supplemental mass for this size buoy was negative in some circumstances and did not follow as smooth a trend as the other hydrodynamic parameters. On the negative side of the chart, the velocity of the buoy did not drop off in a similar fashion with a sinusoidal response of the buoy, rather, the motion became very erratic and that is why the values are essentially flat. This appeared to be the trend for all the buoys when tested at the shortest wave period. The actual velocity response of the hemispherical buoy with a regular wave of period of 6s is seen here in Figure 56.

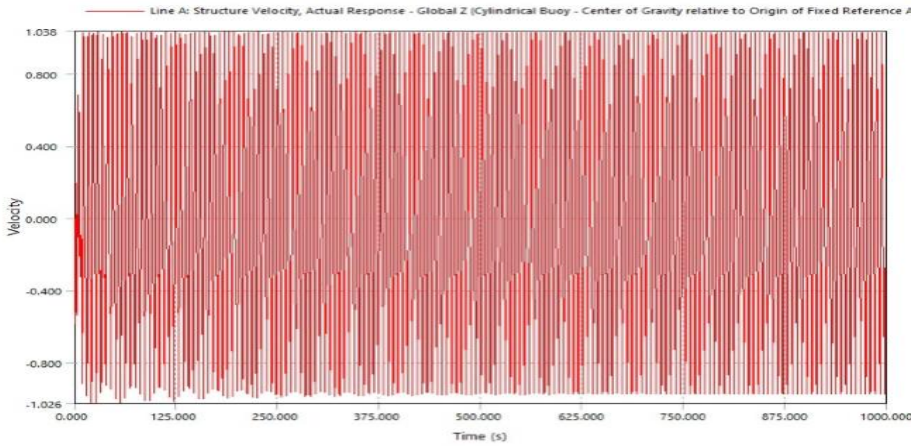

Figure 56. Velocity response for hemispherical buoy under regular wave conditions

The duration of the trial was 1000s to allow the response to stabilize; the velocity of the buoy was sinusoidal and converged around 750s.

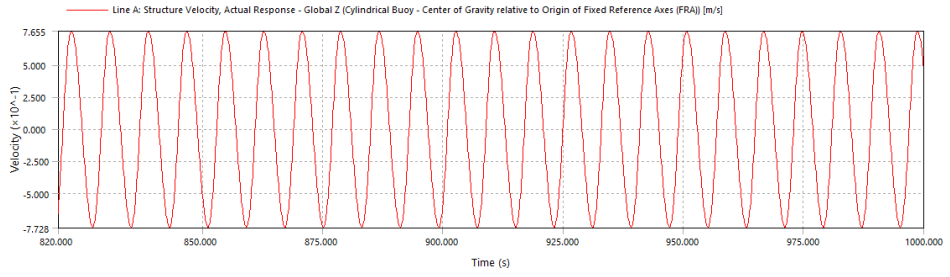

Figure 57. Buoy exhibiting sinusoidal velocity response

Figure 57 is a close-up view of a 120s section of a trial that shows the sinusoidal response of the buoy in response to a regular wave. This is important because it was determined that as the velocity profile became more irregular, there was a point where the velocity began to drop off. Some irregularity in the profile was acceptable because it was determined that as the PTO damping coefficient was introduced, it smoothed out the velocity profile back to a sinusoidal curve. However, when too much damping was implemented the velocity fell off precipitously resulting in a large loss of power. Despite the difficulty in finding the optimized supplemental mass, the response to the added PTO damping was similar in three of the four cases as seen in Figure 58.

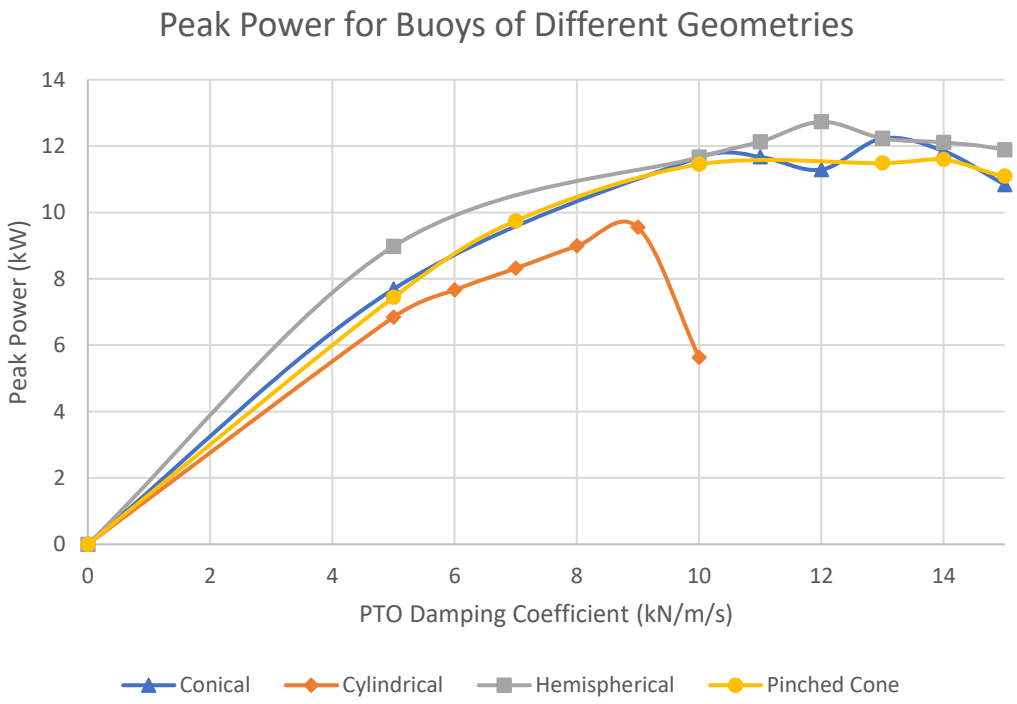

Figure 58. Peak power for different buoy shapes with a diameter of 2.98m

The peak power of the cylindrical buoy however was about 10% less than the other 3 buoy shapes and then dropped off much more quickly. The peak power for the hemispherical buoy was on average slightly higher

than the conical or pinched cone for the 2.98-m buoy. The optimized peak power for the remaining diameters is seen in Figures 59 through 61.

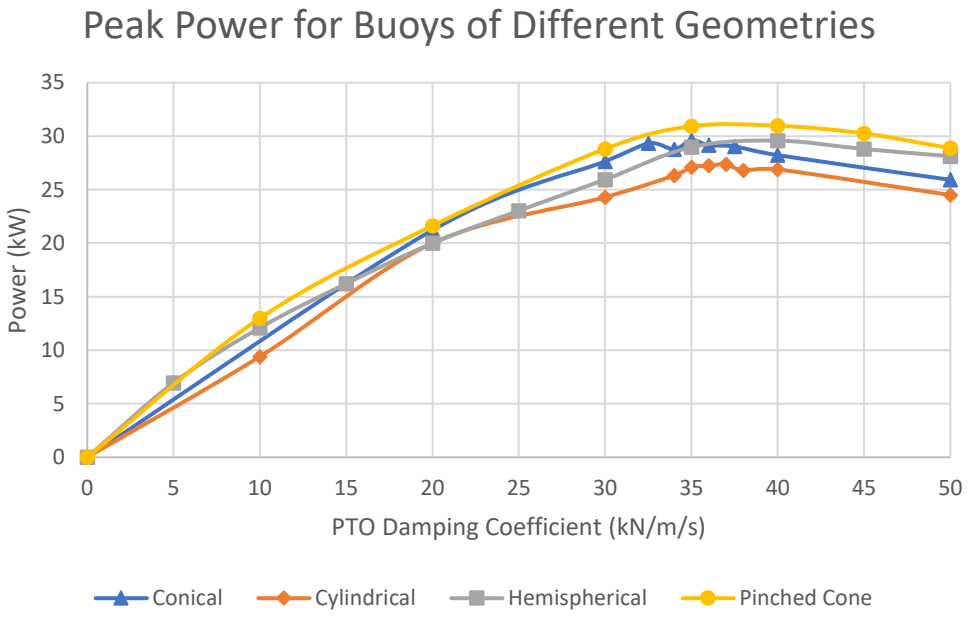

Figure 59. Peak power for different buoy shapes with a diameter of 4.05m

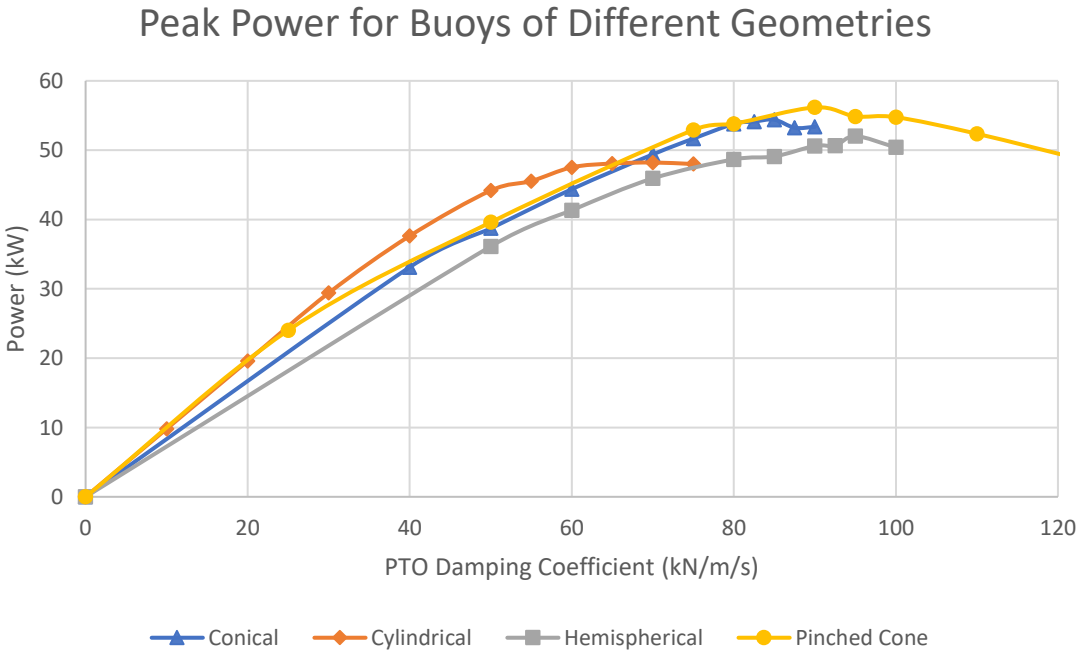

Figure 60. Peak power for different buoy shapes with a diameter of 5.30m

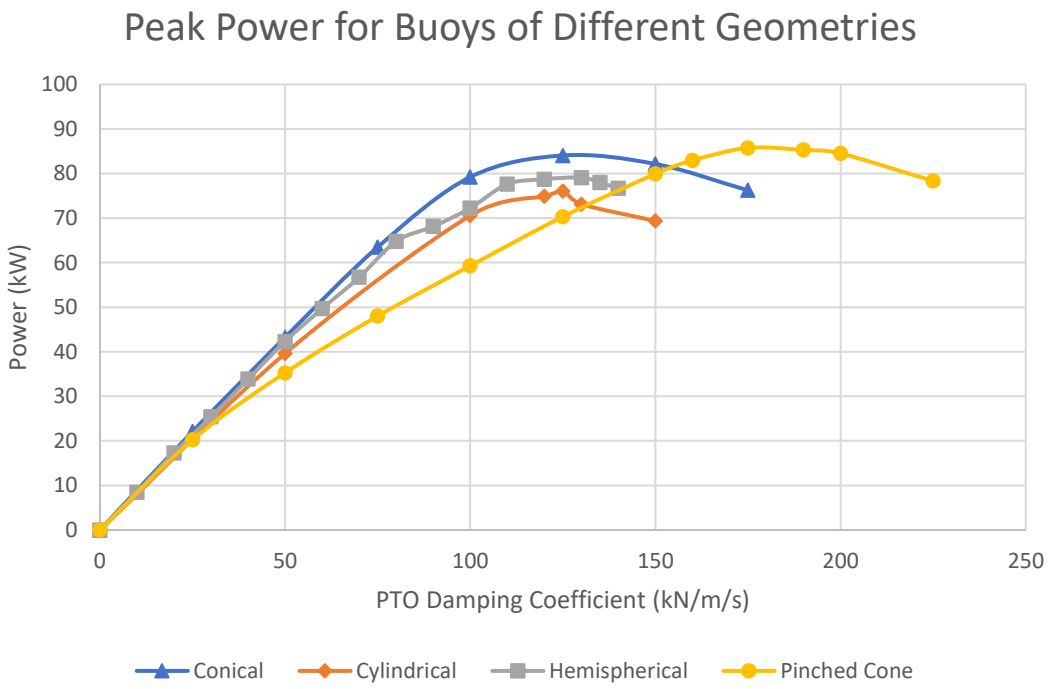

Figure 61. Peak power for different buoy shapes with a diameter of 6.70m

There was some variability in the peak performance of each of the shapes at different diameters. In the case of the smallest diameter, the hemispherical buoy seemed to produce the highest power level but was very closely matched by the conical and pinched cone buoys, within the ten percent margin. The cylindrical buoy produced less, coming in at a value 25% less than the top performer. With the three remaining diameters, there was an increase in peak power output from the pinched cone shape ranging from 10% to 15% over the cylindrical shape. However, each of these shapes must be compared across the entire spectrum of tested wave periods to see the overall trends. Figure 62 shows the overall performance of the different buoy shapes over the range of tested wave periods for the optimized peak power production. This matches quite closely with the trends of the excitation forces in Figures 43-46, indicating the pinched cone buoy had both the highest excitation force and the highest peak power. This is reasonable evidence, at least within the constraints of this study, to claim there is a significant relationship between excitation forces on the oscillating body and the peak power capability.

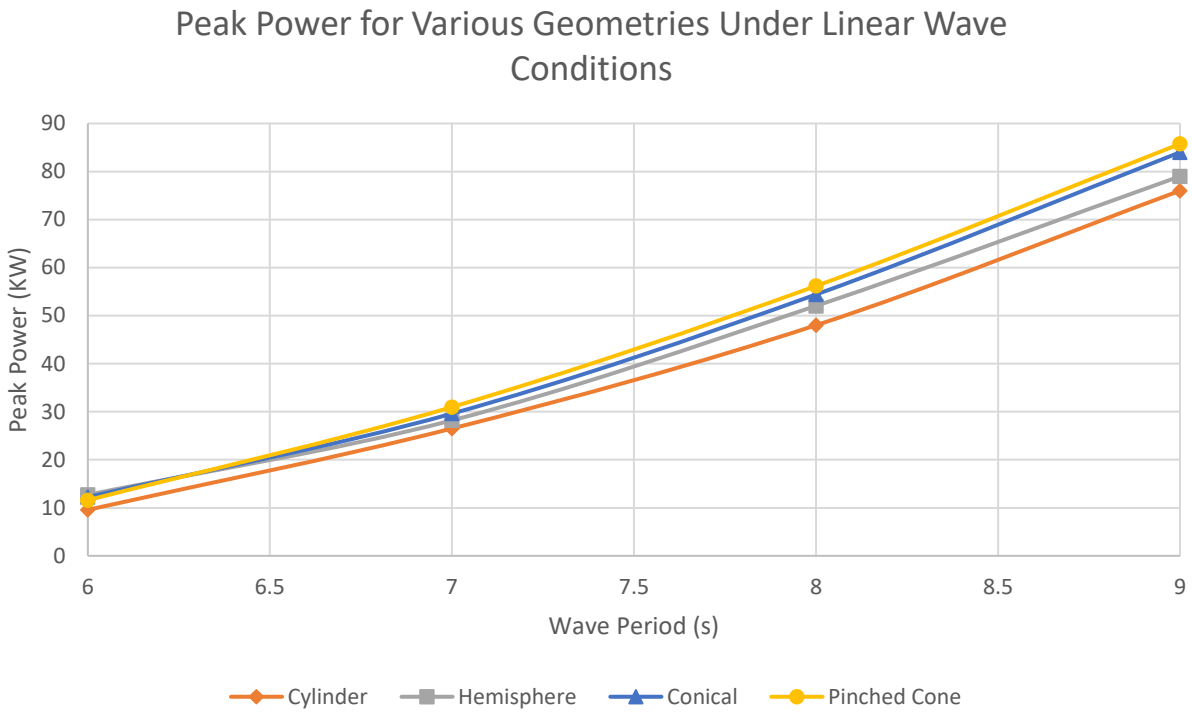

Figure 62. Peak power developed by different shaped buoys over a range of wave periods

Table 3 shows the percentage increase in power across the different periods of the hemispherical, conical, and pinched cone buoys over the cylindrical buoy.

Table 3. Percentage increase in peak power of different shaped buoys over cylindrical buoy

Cylinder		Hemisphere			Conical			Pinched Cone		
Period (s)	Power (kW)	Period (s)	Power (kW)	% diff	Period (s)	Power (kW)	% diff	Period (s)	Power (kW)	% diff
6	9.58	6	12.7	32.57%	6	12.23	27.66%	6	11.5934	21.02%
7	26.5	7	28.2	6.42%	7	29.6	11.70%	7	30.976	16.89%
8	48	8	52.03	8.40%	8	54.4	13.33%	8	56.169	17.02%
9	76	9	79	3.95%	9	84	10.53%	9	85.75	12.83%
			average	12.83%		average	15.80%		average	16.94%

The average increase across all four wave periods exceeded the 10% measure of performance that was proposed. This is an initial indicator that optimizing the geometry as well as the supplemental mass and PTO damping could be worthwhile as the WEC industry continues to develop energy capture devices.

4.6 Time-averaged and instantaneous power

A check on the validity of the data provided is to examine the instantaneous and time-averaged power of the WECs. This may help account for any additional factors that were not identified in the peak power calculations. To do this, a sample of the velocity profile was chosen from each of the responses of 20s towards the very end of the sampling period. This was a sufficient period of time to allow the data points to stabilize and provides a sampling of the data that showed the variation from one peak to the next. Across the sampling after stabilizing, this trend of one higher peak followed by a lower peak was repeated. The instantaneous power was calculated based on the PTO damping coefficient and plotted against a time scale, seen here in Figure 63.

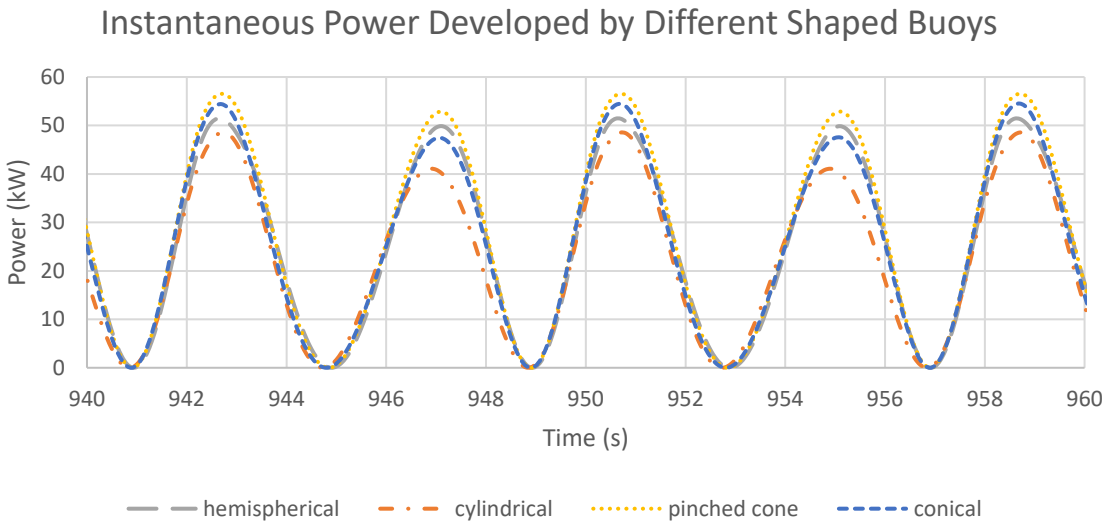

Figure 63. Instantaneous power from buoys of different geometry with a diameter of 2.98m

Additionally, the time-averaged power was calculated over the entirety of the sampling period after each of the trials stabilized. To make the comparison, one diameter of the set of buoys is examined for a regular wave. Table 4 shows that the percentage increase in time-averaged power is over 10% for each of the shapes compared to the cylindrical buoy for the selected buoy size.

Table 4. Time-averaged power of different buoys with a diameter of 5.30m

Time Averaged Power (kW)						
Cylindrical	Hemispherical	% diff	Conical	% diff	Pinched Cone	% diff
22.53	25.43	12.87%	25.53	13.32%	27.36	21.44%

The validation of the increase in power capture capability by calculating time-averaged power shows that there appears to be a benefit to optimizing the geometric shape of the buoy.

4.7 Response of optimized design in irregular waves

The last portion of the experiment was to examine the effects of an irregular wave on the power capture capability of the devices to see if the relationship still existed where there was a clear advantage of one geometric shape over another. To do this, the Aqwa solver was used again with a change in the analysis type of the hydrodynamic response to irregular wave and was set up with the conditions of the wave as previously described. This entails selection of the JONSWAP (H_s) wave spectrum and setting up the amplitude, peak period, and gamma peak enhancement factor. The duration of the analysis was the same as for the irregular wave, 1000s, and the results proved to be significantly different. Figure 65 is the velocity profile of the 2.98-m diameter conical buoy when impinged upon by an irregular wave with a peak period of 6s and significant wave height of 1m.

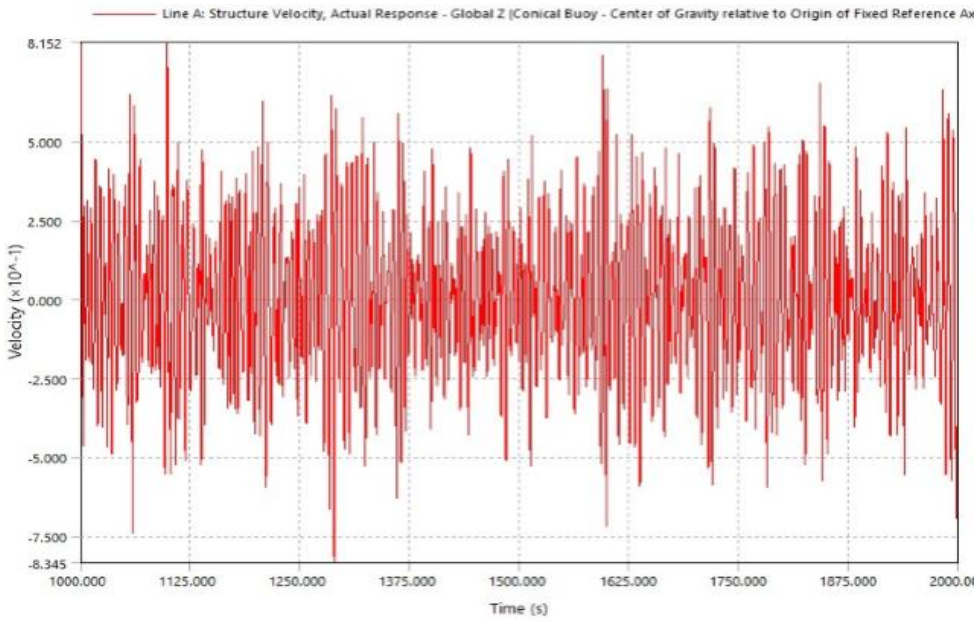

Figure 64. Conical buoy velocity profile in response to an irregular wave

The velocity response of the buoy was significantly affected by the difference in wave type, as compared to the response in regular waves. When the velocity profile was multiplied by the PTO damping coefficient the resulting average power was 0.74 kW. This is in contrast to the 5.63 kW time-averaged power produced by the same buoy under regular wave conditions. The cylindrical buoy produced 0.70 kW. The hemispherical buoy produced 0.027 kW. The pinched cone buoy produced 0.012 kW. This result has no correlation to the equivalent regular wave response and does not support the hypothesis that the improvements found with the pinched cone buoy can translate over to the irregular wave response. Further experimental data is required to better understand these results and move forward.

CHAPTER 5

CONCLUSIONS AND FUTURE WORK

In this experiment, the relatively immature field of wave energy conversion is further explored as an alternative method for producing energy in support of America's expanding energy portfolio. Regardless of the evidence for or against the availability of natural resources to power today's society for many years to come, the simple fact is that at some point in the not-too-distant future, non-renewable resources may run out if changes aren't made. If it is the intent to maintain a good quality of life, then it is imperative to lean forward now to develop those technologies further that will allow it.

There are thousands of patents for wave energy devices. Because of the intermittent nature of waves and the variability across the globe of different sea states, it is extremely challenging for researchers and scientists to pin down the best way to harness the power of the ocean waves. The success of point absorber wave energy devices has been exhibited on a small scale in places like the U.K., China, and the U.S. This experiment attempts to build off those successes and improve the understanding of the capacity of axisymmetric buoys to capture wave energy. The hydrodynamic parameters of a floating body have been determined as a way to solve the equation of motion for an oscillating body in the heave direction, and those parameters which are frequency and shape dependent can be solved rapidly using a commercially available software such as ANSYS Aqwa. The solver can then utilize those parameters and the principles of linear wave theory using small amplitude waves in deep water to solve for the forces acting on the oscillating body and the response to those forces.

In this experiment, four different models of an axisymmetric buoy were designed and tested, each with a different bottom shape. The diameter and draft of the buoys were designed based on criteria previously established in wave energy research and the shapes tested were chosen based upon certain assumptions about the relationship between power capture and excitation forces. Each buoy was tested using the Aqwa Hydrodynamic Response solver and the parameters and response were found over a range

of frequency and wave types. The hydrodynamic parameters of excitation force, radiation damping coefficient, and added mass were all analyzed for each buoy shape and diameter. The excitation forces increased dramatically with increasing buoy diameter as well as frequency.

The power capture capability of each device was analyzed in a way that attempted to isolate the changes in geometry as the defining factor for the test. Each buoy was optimized at every level using an iterative optimization process. This process was cross checked against other methods and found to produce reasonable and repeatable results. Once the supplemental mass was found that produced the maximum peak velocity for a buoy, an external PTO damping coefficient was introduced to simulate a power capture device. The level of PTO damping was increased until a peak power was identified. This power was then compared across all the devices.

Under regular wave conditions, it was determined that there was between a 12% and 17% increase in the peak power capture of the devices with a modified shape compared to a regular cylindrical buoy. A sampling of the time-averaged power of one of the devices was also compared to the cylindrical buoy and an improvement in performance was even more significant. It was determined that a more significant difference resulted from buoys of lesser diameter in waves of shorter wave period. These results supported the hypothesis that the geometric shape of an axisymmetric buoy could be optimized for higher performance and may provide the motivation for further development of buoys with a pinched cone shape.

Unfortunately, when the buoys were evaluated in their response to irregular waves, the results were not supportive of the hypothesis. Not only was the power capture of the devices orders of magnitude less, but the geometric shape of the buoys and respective power capture when compared to a cylindrical shape no longer reflected improved performance. This indicates that more work is needed to identify the information gaps in the irregular wave tests. Previous research has identified that a concentration on the predictive control of damping could result in big power gains by changing the PTO damping for the device for every incoming wave. However, this does not account for the optimization of the added mass, which was found to be equally important in the development of an effective power capture device.

Throughout this experiment, an increased understanding of the interaction between waves and oscillating bodies has been developed. The field of wave energy continues to fascinate researchers around the world, however, it will still be many years before the goal of reducing or eliminating human's carbon footprint can be achieved. Even after fully embracing the pursuit of wave energy technology along with the all the other renewable methods currently in use, there are a myriad of issues still to tackle. From shifting political climates to massive infrastructure changes, the obstacles are many, but the reward will be immense. The exploration into the geometric optimization of point absorber wave energy converters has uncovered some new ideas but also some new questions as a result of this experiment. With further research and testing, these devices will continue to improve and move into the next stage of commercial development. Future work as a result of this experiment will be to continue the development of the optimization process with the use of computational fluid dynamics to better model complex sea states. The modeling and analysis of a point absorber WEC can be accomplished using the ANSYS application Fluent, whereby the lift and drag coefficients can be determined and the velocity profiles can be generated with respect to time. These results can then be compared to real world experiments on models in wave tanks and then at full scale. Applications of wave energy converters will include wave energy farms that can be tied into an existing electrical grid. Economies of scale can be applied in such a way as to make the LCOE of wave energy within reach of other currently available alternative energy options. Additionally, single unit devices can be developed that can provide rapidly deployable point generation and possibly create easily accessible power for coastal or island communities that have been struck by natural disasters. The possibilities for wave energy converters are endless and the next 10 to 20 years will be a very exciting time to see how it all develops.

Appendix A. Linear Wave Theory Basic Relationships and Nomenclature

Wave Property	Deep Water ($\frac{h}{\lambda} > \frac{1}{2}$)	legend
Velocity Potential $u = \nabla\phi$	$\phi = \frac{ag}{\omega} e^{kz} cos(\omega t - kx)$	$\omega = \frac{2\pi}{T}$ $k = \frac{2\pi}{\lambda}$ T = wave period λ = wavelength a = wave amplitude g = acceleration of gravity $c = \frac{\lambda}{T}$ = phase speed t = time h = water depth
Dispersion Relation	$\omega^2 = gk$	
Wave Length/Wave Period Relationship	$\lambda = \frac{g}{2\pi} T^2$	
Wave Profile	$\eta = asin(\omega t - kx)$	
Group Velocity	$c_g = \frac{1}{2} c$	

REFERENCES

1. Barnola J, Raynaud D, Korotkevich Y, Lorius C. 1987. Vostok ice core provides 160,000-year record of atmospheric CO_2. Nature 329: 408-14.

2. Bent R, Orr L, and Baker R. 2002. Energy: Science, Policy, and the Pursuit of Sustainability. Institute for Advanced Study, Indiana University. Washington, DC: Island Press.

3. Borowitz S. 1999. Farewell Fossil Fuels: Reviewing America's Energy Policy. New York: Plenum Press.

4. Charlier R, Justus J. 1993. Ocean Energies: Environmental, Economic and Technological Aspects of Alternative Power Sources. Amsterdam: Elsevier Publishing.

5. Cummins W. 1962. The impulse response function and ship motions. Research and Development Report. Department of the Navy. Hydromechanics Laboratory.

6. De Backer G. Hydrodynamic design optimization of wave energy converters consisting of heaving point absorbers. PhD Dissertation. Ghent University.

7. Falnes J. 2004. Ocean Waves and Oscillating Systems. Linear Interactions Including Wave Energy Extraction. Edinburgh, England: Cambridge University Press.

8. Fanchi J. 2004. Energy: Technology and Directions for the Future. Burlington, MA: Elsevier Academic Press.

9. Gaunche R, Gomez V, Vidal C, Eguinoa I. 2013. Numerical analysis and performance optimization of a submerged wave energy point absorber. Ocean Engineering 59: 214-230.

10. Ghasemi A, Anbarsooz M, Malvandi A, Ghasemi A, Hedayati F. 2017. A nonlinear computational modeling of wave energy converters: a tethered point absorber and a bottom-hinged flap device. Renewable Energy 103: 774-785.

11. Hager R. 2012. Geometric effects on maximum power absorption efficiency for a single, two-dimensional heaving body. Master's Thesis. University of Hawaii. August 2012.

12. Hakes J. The Road to America's First Energy Crisis: New Insights on the Growing Weakness of the United States as a Global Energy Power, 1967-1973.

13. Hartnett J. 1976. Alternative Energy Sources. New York, New York: Academic Press.

14. Hasselmann K, Barnett T, Bouws E, Carlson H, Cartwright D, Enke K, et al. 1973. Measurements of wind-wave growth and swell decay during the joint north sea wave project. German Hydrographic Institute. Hamburg, Germany.

15. International Towing Tank Conference. 2014. Wave energy converter model test experiments.

16. Kelley J. 2017. A Clean Energy's Dirty Little Secret. Available: https://www.nationalreview.com/2017/06/solar-panel-waste-environmental-threat-clean-energy/. [accessed 23 May 2018].

17. Krogstad H, Arntsen O. 2000. Linear Wave Theory, Part A: Regular Waves (Draft). Norwegian University of Science and Technology. Trondheim, Norway.

18. Kweon H, Cho H, Cho I. 2014. A study on the optimum draft of multiple resonance power buoys for maximizing electric power production. International Journal of Naval Architecture and Ocean Engineering 6: 813-825.

19. Le Méhauté B. 1976. An Introduction to Hydrodynamics and Water Waves. Springer Study Version. Heidelberg, Germany: Springer Publishing.

20. Lewis E. 1989. Principles of Naval Architecture, Second Revision, vol. 3: Motions in Waves and Controllability. Jersey City, NJ: The Society of Naval Architects and Marine Engineers.

21. Mapping and Assessment of the United States Wave Energy Resource. EPRI. Palo Alto, CA: 2011.1024637. 2011.

22. Mørk G, Barstow S, Kabuth A, Pontes M. 2010. Assessing the global wave energy potential. In: Proceedings of the 29th International Conference on Ocean, Offshore Mechanics and Arctic Engineering, June 2010, Shanghai, China.

23. Mott R. 2000. Applied Fluid Dynamics, 5th Edition. Upper Saddle River, New Jersey: Prentice-Hall Inc.

24. NASA. 2018. Global Climate Change. Available: https://climate.nasa.gov/evidence/ [accessed 12 September 2018].

25. National Weather Service. 2018. Significant wave height. Available: https://www.weather.gov/key/marine_sigwave [accessed: 16 OCTOBER 2018].

26. NERACOOS (Northeastern Regional Association of Coastal Ocean Observing Systems). 2018. Hourly Buoy Data from the coast of Maine. Available: http://www.neracoos.org/datatools/historical/graphing_download [accessed 27 September 2018].

27. Palm J, Eskilsson C, Paredes G, Bergdahl L. Coupled mooring analysis for floating wave energy converters using CFD: formulation and validation. International Journal of Marine Energy 16: 83-99.

28. Pastor J, Liu Y. 2014. Frequency and time domain modeling and power output for a heaving point absorber wave energy converter. International Journal of Energy and Environmental Engineering 5: 101.

29. Penalba M, Sell N, Hillis A, Ringwood J. 2017. Validating a wave-to-wire model for a wave energy converter-part I: the hydraulic transmission system. Energies Magazine 10: 977–999.

30. Penalba M, Touzon I, Lopez-Mendia J, Nava V. 2017. A numerical study on the hydrodynamic impact of device slenderness and array size in wave energy farms in realistic wave climates. Ocean Engineering 142: 224-232.

31. See P, Tai V, Molinas M. 2012. Ant colony optimization applied to control of ocean wave energy converters. Energy Procedia 20: 148-155.

32. Shadman M, Estefen S, Rodriguez C, Nogueira I. 2018. A geometrical optimization method applied to a heaving point absorber. Renewable Energy 115: 533-546.

33. Siddique M. 2018. Chapter 2: Waves and Tides. PowerPoint Presentation. University of Sharjah. Dept. of Civil and Environmental Engineering. Available: https://www.slideshare.net/yourmohsin/chapter-2-wave-and-tides [accessed 9/27/2018].

34. Sjokvist L, Goteman M, Rahm M, Waters R, Svensson O, Stromstedt E, et al. 2017. Calculating buoy response for a wave energy converter-a comparison of two computational methods and experimental results. Theoretical and Applied Mechanics Letters 7: 164-168.

35. Sjokvist L, Krishna R, Rahm M, Castellucci V, Hagnestal A, Leijon M. 2014. On the optimization of point absorber buoys. Journal of Marine Science and Engineering 2: 477-492.

36. Sokolowski J, Banks C. 2009. Principles of Modeling and Simulation: A Multidisciplinary Approach. Hoboken: John Wiley & Sons, Inc.

37. Stansby P, Moreno E, Stallard T. 2015. Capture width of the three-float multi-mode multi-resonance broadband wave energy line absorber M4 from laboratory studies with irregular waves of different spectral shape and directional spread. Journal of Ocean Engineering and Marine Engineering 1: 287-298.

38. Stegman A, Andres A, Jeffrey H, Johanning L, Bradley S. 2017. Exploring marine energy potential in the U.K. using a whole systems modelling approach. Energies 10: 1251-1271.

39. United States Department of Energy. 2017. Lawrence Livermore National Laboratories. Estimated U.S. Energy Consumption in 2017. Available: https://flowcharts.llnl.gov/ [accessed] 16 May 2018.

40. United States Census Bureau. 2018. World Population Clock. Available: https://www.census.gov/popclock/ [accessed 16 May 2018].

41. United Nations Department of Economic and Social Affairs, Population Division. 2017. World Population Prospects: The 2017 Revision, Key Findings and Advance Tables. ESA/P/WP/248.

42. United Nations Development Programme. 2016. Human Development Report 2016.

43. United States Department of Energy. National Renewable Energies Lab. 2018. Solar Energy Potential. Available: https://www.energy.gov/maps/solar-energy-potential/. [accessed 23 May 2018].

44. United States Department of Energy. National Renewable Energies Lab. 2018. Wind Resource Map. Available: http://rredc.nrel.gov/wind/pubs/atlas/maps/chap2/206m.html/ [accessed 21 May 2018].

45. United States Energy Information Administration, Office of Energy Analysis, Department of Energy. 2018. Annual Energy Outlook 2018.

46. United States Energy Information Administration, Department of Energy. 2018. Levelized Cost and Levelized Avoided Cost of New Generation Resources in the Annual Energy Outlook.

47. Victoria C. 2018. The History of Solar Power. Available: https://www.experience.com/advice/careers/ideas/the-history-of-solar-power/ [accessed 23 May 2018].

48. Wired Magazine Online. 2018. America's Wind Energy Potential Triples in New Estimate. Available: https://www.wired.com/2010/02/better-wind-resource-maps/ [accessed 21 May 2018].

49. World Energy Council. 2016. World Energy Resources: Marine Energy 2016.

50. Youssef J, Matar J, Rahme P, Bou-Mosleh C. 2016. A nearshore heaving-buoy sea wave energy converter for power production. In: Proceedings of International Conference on Sustainable Design, Engineering, and Construction. Procedia Engineering 145: 136-143

51. Zang Z, Zhang Q, Qi Y, Fu X. 2018. Hydrodynamic responses and efficiency analysis of a heaving-buoy wave energy converter with PTO damping in regular and irregular waves. Renewable Energy 116: 527-542.